TU Delft

Delft University of Technology

Document Version
Final published version

Licence
CC BY-NC-ND

Citation (APA)
Yang, C., Abdelrahman, M., Khaloian-Sarnaghi, A., & van de Kuilen, J. W. (2025). A comprehensive analysis of fatigue in wood and wood products. *International Journal of Fatigue*, *194*, Article 108807. https://doi.org/10.1016/j.ijfatigue.2025.108807

Important note
To cite this publication, please use the final published version (if applicable).
Please check the document version above.

Copyright
In case the licence states “Dutch Copyright Act (Article 25fa)”, this publication was made available Green Open Access via the TU Delft Institutional Repository pursuant to Dutch Copyright Act (Article 25fa, the Taverne amendment). This provision does not affect copyright ownership.
Unless copyright is transferred by contract or statute, it remains with the copyright holder.

Sharing and reuse
Other than for strictly personal use, it is not permitted to download, forward or distribute the text or part of it, without the consent of the author(s) and/or copyright holder(s), unless the work is under an open content license such as Creative Commons.

Takedown policy
Please contact us and provide details if you believe this document breaches copyrights.
We will remove access to the work immediately and investigate your claim.

This work is downloaded from Delft University of Technology.

International Journal of Fatigue 194 (2025) 108807



Contents lists available at ScienceDirect

International Journal of Fatigue

journal homepage: www.elsevier.com/locate/ijfatigue



A comprehensive analysis of fatigue in wood and wood products

Changxi Yang [a,1,*], Mostafa Abdelrahman [a,b,1], Ani Khaloian-Sarnaghi [a], Jan-Willem van de Kuilen [a,c]

[a] Department of Materials Engineering, Technical University of Munich, Winzererstrasse 45, Munich, 80797, Bavaria, Germany
[b] Department of Civil Engineering, Suez Canal University, 4.5 Km the Ring Road, Ismailia, 8366004, Egypt
[c] Department of Engineering Structures, Delft University of Technology, Stevinweg 1, Delft, 2628, The Netherlands

ARTICLE INFO

Keywords:
Fatigue
Wood
S–N curve
Viscoelasticity
Failure mechanism

ABSTRACT

Fatigue failures pose significant challenges across various engineering disciplines. Wood, due to its low carbon emissions and high strength-to-weight ratio, has been gaining attention in engineering applications. The fatigue behavior of wood is complex due to its heterogeneous, anisotropic, and viscoelastic nature. This research explores essential insights into the fatigue behavior of wood, with a focus on S–N curves, stress–strain behavior, and failure mechanisms. Due to often varying failure criteria and test settings, direct comparison of S–N curves across different studies can be challenging and inconclusive. A closer look shows that wood in fatigue shows both irreversible and recoverable strain components that are delayed. However, there have been conflicting reports about residual stiffness changes under fatigue loading. Theoretical fatigue life models based on S–N curves or duration of load theory have shown limited applicability. Efforts to develop progressive damage model based on stress–strain behaviors have been challenging and largely unsuccessful due to the lack or inconsistency of data. Understanding the microstructural failure mechanism is crucial in order to build a more trustworthy fatigue modeling technique. Further work is suggested to monitor the microstructural deterioration during high-cycle fatigue loading.

1. Introduction

Wood has been an essential material for human civilization, used in applications from simple shelters and sport goods to musical instruments and complex architectural structures. Its natural abundance, ease of workability, and aesthetic appeal have made it a preferred choice for construction engineers and craftsmen throughout history. However, like all materials, wood is subject to degradation over time, with fatigue being a significant factor that can affect its structural integrity.

Fatigue of wood was generally not considered as a crucial design parameter. The fact that trees can withstand millions of cycles wind storms during its natural growth process made early workers overestimate the fatigue resistance of wood. Barlow [1] noted that "Fatigue in properly seasoned wood is unknown", which represents the common belief that has led to the widespread use of wood in bombers and troop gliders. It was until World War II that growing concerns prompted serious investigations into fatigue of wood [2].

Beyond the interest from the aircraft industry, structural engineers have also recognized the importance of fatigue in timber structures. While cyclic stresses in timber structures are generally low and do not typically lead to significant fatigue failures, certain scenarios require careful consideration. For example, fatigue can be a critical design factor in road bridges and wind turbines. Road bridges are constantly subjected to the weight of passing vehicles, with heavy trucks or trams posing particular challenges. The interest in fabricating wind turbine blades from laminated wood emerged during the 1970s and 1980s [3,4]. Wind turbine blades are mainly subjected to varying wind loads and rotational gravity forces. Moreover, severe reversed loading may also occur at timber joints of roof structures, during storms or earthquakes.

In contrast to monotonic tests, fatigue investigations are inherently more complicated due to the numerous fatigue parameters involved in the testing procedure. For constant-amplitude fatigue tests, the stress level (SL) – quotient between the applied stress and the ultimate short-term strength – generally determines the total number of cycles that the material can sustain. The mean SL, reflected in the R ratio (lowest to highest SL), also affects fatigue life. Negative R values signify reversed fatigue loading, which has been proven as a more severe case than repetitive fatigue loading for wood [3,5].

Wood is an heterogeneous material with varying properties in different directions. Sensitivity to environmental conditions, particularly to moisture content, results in hygroexpansion and the so-called mechanosorption, significantly affecting the mechanical response of

* Corresponding author.
E-mail address: changxi.yang@tum.de (C. Yang).
[1] The authors contributed equally to this work.

https://doi.org/10.1016/j.ijfatigue.2025.108807
Received 28 October 2024; Received in revised form 17 December 2024; Accepted 3 January 2025
Available online 22 January 2025
0142-1123/© 2025 The Authors. Published by Elsevier Ltd. This is an open access article under the CC BY-NC-ND license (http://creativecommons.org/licenses/by-nc-nd/4.0/).

Nomenclature

low-cycle fatigue	The material is subjected to high stress magnitude and failure occurs within 10^5 load cycles.
high-cycle fatigue	The material is subjected to low stress magnitude and sustains more than 10^5 load cycles.
repeated fatigue	The cyclic stress does not change direction.
reversed fatigue	The sign of cyclic stress changes.
hysteresis loop	The stress–strain response of the material during one load cycle.
fatigue strain	The total accumulated strain measured at the maximum stress of a load cycle.
residual strain	The strain that is not immediately recoverable after unloading.
residual stiffness	The stiffness during fatigue loading or (and) unloading phase.
waveform	The shape of the stress–time curve, including sinusoidal, square, trapezoidal, triangular, or sawtooth waves.

Symbols

σ_p	Peak stress, the highest stress value within a load cycle.
σ_v	Valley stress, the lowest stress value within a load cycle.
$\sigma_{\max}$	Maximum stress, the highest absolute stress value within a load cycle.
$\sigma_{\min}$	Minimum stress, the lowest absolute stress value within a load cycle.
σ_m	Mean stress, the average value of σ_p and σ_v.
σ_a	Stress amplitude, the difference between σ_m and σ_p.
R	The ratio between σ_v and σ_p ($R = \sigma_v/\sigma_p$). In pure compression cases: $1 < R \leq \infty$; in pure tension cases: $0 \leq R < 1$.
f	Frequency, the number of load cycles per second (in [Hz]).

Abbreviations

SL	Stress level, the ratio between $\sigma_{\max}$ and ultimate short-term strength of the material.
NOC	Number of loading cycles.

wood. Moreover, wood exhibits viscoelastic behavior and thus delayed load effects. As a consequence, the fatigue life of wood can be also influenced by excitation frequency and the applied load waveform [6]. Last but not least, the microstructure of wood – including growth rings and defects such as knots and fiber deviations – affects fatigue crack initiation and propagation. These combined factors make fatigue testing and modeling for wood more intricate, requiring advanced methods to account for its unique properties and to predict its mechanical response.

The fatigue behavior of wood and its modeling has been the objective of numerous researches. Smith et al. [7] provided an overview on general experimental observations on fatigue life and failure mechanism of wood. A more detailed review specifically addressing the bending fatigue of wood has been provided by Tsai & Ansell [3]. Gong [8] summarized a large number of experimental observations on fatigue of wood, which contain also uniaxial fatigue tests. Apart from uniaxial loading and bending, efforts to examine shear, torsion, or combined loading conditions have been relatively scarce [9–16]. Fatigue properties of wood laminate and wood-based panel products have been reviewed by Ansell [4]. In recent years, fatigue performance of adhesives and wood joints has been a focus of research [17–25].

Conclusions about wood fatigue are largely based on S–N curve analysis. The EN 1995-2-2 (Annex A) [26] distinguishes compression, tension, shear, dowel and nail cases and applies S–N curves proposed by Malo et al. [27] for design guidance. While certain fatigue parameters such as R ratio have been considered in the proposed S–N curves, Malo et al. [27] commented that the proposed general curve can have limited feasibility in certain ranges. In fact, the complex interplay between different fatigue parameters, such as between frequency and R ratio, makes it difficult to draw quantitative conclusions from comparing S–N curves at different test conditions. So far, a general mathematical form of S–N curve that integrate all fatigue parameters has not been derived. Additionally, important aspects such as stress–strain behavior and property changes during fatigue loading remain largely underexplored.

Therefore, this paper aims to give a up-to-date and complete analysis on the available fatigue research in wood, helping to establish a fundamental understanding of the fatigue mechanism. The paper is structured as follows:

- Section 2 covers essential conclusions drawn from S–N curve and discusses experimental setups that may influence those conclusions;
- Section 3 compares S–N curves from the most relevant literature and discusses different fatigue parameters;
- Section 4 highlights the stress–strain behavior of wood during cyclic loading, addressing viscoelasticity and property changes during fatigue loading;
- Section 5 summarizes empirical fatigue models of wood, emphasizing the different failure criteria;
- Section 6 provides a synthesis of findings in fracture morphology and failure mechanism of wood in fatigue, highlighting microscopic investigations on fatigue failure mechanism of wood.

The emphasis is on uniaxial loading and bending cases, since the majority of researches are covered by these loading types. Knot-free solid wood and wood-based products are discussed. Effects of environmental conditions such as temperature and moisture content are also excluded.

2. S–N curve

The S–N curve is a practical measurement of fatigue resistance and has been the primary focus of most research on wood fatigue. In constant-amplitude fatigue tests of wood, the applied SL is plotted against the corresponding NOC to failure, typically resulting in a near-linear curve when plotted on a semi-logarithmic axis. The following subsections contain essential observations from S–N curves and examine key experimental aspects to help establish a better understanding of S–N curves.

2.1. Endurance limit

The endurance limit is one of the first information delivered by S–N curves. The endurance limit refers to the SL that is low enough to avoid any failure even if loaded to an infinite NOC.

Several early studies on parallel-to-grain bending and tension seemed to reveal an endurance limit. Although the reported endurance limit in literature varied slightly among different species and test conditions, an approximate range of 22% to 36% was kept consistent for all investigated cases [28–32]. Only Lewis [33] reported a much higher bending endurance limit of 50%. However, Lewis' study was conducted on large-scale specimens that may contain knots. Therefore, the results may not be completely comparable to the previously mentioned literature.

Most of the abovementioned researchers considered the test as reaching an endurance limit, if a number of runouts occurred at a certain SL. "Runouts" occur when the test has to be suspended before specimen failure due to either time or equipment constraints. However, including runouts simply to the S–N curve may add false information

to the shape and mathematical form of S–N curves [34]. The mechanical properties of wood vary from tree to tree and from specimen to specimen. Even selecting specimens in a way to cover similar density, year ring width and stiffness value, may result in "un-identical" short-term strength. As a consequence, the possibility of runouts occurring simply as a result of sample scattering cannot be excluded. For attempts to statistically deal with runouts in wood fatigue tests, the reader is referred to the work by Dean [35], Klemenc & Fajdiga [36], or Clerc [23].

To exclude the influence of sample scattering in those runouts, the fatigue test would have to be continued to a much longer time span. In practice, however, reaching infinite NOC is impossible. A range of 1 to 10 million cycles are generally considered sufficient to determine the endurance limit [28,33,37]. The bending and compression test at 57.5 Hz by Fuller & Oberg [37] was the only study available to the author that continued fatigue testing until exceeding 100 million NOC. The results also confirmed that solid wood specimens subjected to bending could survive 100 million at a SL of 27.6%.

Indirect evidence for endurance limit has been achieved by measuring the extent of "damage" in fatigue-tested specimens. If one assumes that fatigue failure is related to some sort of "damage" that accumulates with NOC, it is logical to infer that an endurance limit is equivalent to the SL that does not cause any "damage" even after millions of load cycles. Efforts have been made to find different indicators for such "damage". Kraemer [28] made the hypothesis that the previous fatigue loading at endurance limit should not influence the fatigue performance of the same specimen subjected to a subsequent higher SL. He found that the data of retested specimens fit the original S–N curve well. Gillwald [38] considered the delayed strain increase as a "damage" indicator. It was observed that there was no visible strain increase for specimens loaded at a SL lower than the assumed endurance limit, even after half a million NOC.

Although the abovementioned observations seemed to enhance the existence of endurance limit for 1 to 10 million NOC, the reader should consider that all literatures mentioned here were conducted with a relatively high loading frequency of over 20 Hz (test frequency was not recorded in Kollmann [29]). The consequence of high loading frequency is twofold. On the one hand, due to the viscoelastic nature of wood, the higher loading rate results in higher strength property and thus lower strain responses. On the other hand, it might also cause high adiabatic heating, potentially leading to moisture content loss and hence lower actual SL and longer fatigue life [3].

Multiple researches discussed about adiabatic heating with relatively high loading frequency. Nakano [39] reported a temperature rise exceeding 10 °C during bending tests at 30 Hz, measured between 1000 and 10,000 NOC. Okuyama & Marsoem [40] suggested a positive correlation of temperature rise with the loading frequency. Furthermore, several researchers have confirmed a certain extent of moisture content loss after fatigue testing. For bending tests, Kraemer [28] and Kommers [32] reported an average moisture content loss of 1%–2% at positions near fatigue failure, with a loading frequency of 50 Hz and 30 Hz, respectively. For uniaxial fatigue tests, Rose [41] reported that the moisture content loss over three million NOC at 40 Hz can be up to 2%, corresponding to an increase of 15 °C in temperature. A similar range of moisture content loss was reported by Kufner [42] in a follow-up test. Moreover, the temperature increase was found to positively correlate to the SL [40,41]. Clorius [43] compared compressive fatigue tests at 0.1 Hz, 1 Hz and 10 Hz, and concluded that the adiabatic heating and moisture content loss was negligible up to 1 Hz.

2.2. Reference short-term strength for fatigue testing

The ultimate short-term strength plays an important role in S–N curves, as it forms the basis for determining the SL. Comparison between S–N curves from different literatures only becomes valid when the ultimate short-term strength was determined on the same basis. This can be particularly critical for compressive tests perpendicular to the grain, where different standards vary significantly in specimen configurations and support lengths. These differences can lead to variations in short-term strength measurements by as much as twofold [44].

The most common way of determining the short-term strength is to take either the mean or a characteristic value of multiple static tests conducted on specimens from the same group. The author did not identify literature that explicitly claimed the use of characteristic short-term strength in fatigue tests. The determination of characteristic values generally requires large number of specimens. If not addressed in the original literature, it is reasonable to assume that the mean value was taken as a reference. Kraemer [28], for instance, took the mean strength of three to four specimens subjected to static loading. It was commented that the scattering was largely reduced through careful selection based on density, moisture content, latewood percentage and year ring width.

In contrast, Gong [8] applied a one-to-one sample matching technique. Specimens were cut in end-to-end pairs, where one specimen was used to determine the short-term strength, which served as the base for the fatigue test conducted on the other specimen. However, as Hunt [45] stated, even well-matched samples may exhibit a standard deviation of ±15% of the mean value. Gong [8] observed that after 120 NOC of fatigue loading at 0.2 Hz, the residual compressive strength of spruce was all higher than the original reference short-term strength. This observation is somewhat counterintuitive, considering that the applied SL ranged between 75% and 95%. The possibility of sample scattering related to the applied sample matching scheme cannot be excluded. Another example of using matched samples can be found in Bach [46], where the exact matching criteria were not clearly stated.

Ogawa et al. [47] applied a density-based "sample matching" technique. By correlating short-term strength with density, they calculated the reference strength value individually for each specimen. Similar to the previous sample matching used by Gong [8] and Bach [46], this method significantly complicates the test process by producing varying stress values for different specimens.

The different loading rates in short-term strength tests are a further aspect that may cause deviations in test results. Tsai & Ansell [3] proved experimentally that the average short-term strength can vary by up to 30% if the stress rate is increased from 1 MPa/s to 1000 MPa/s, depending on the species. They suggested that in order to get accurate reference strength values, the short-term strength tests should use a comparable, if not identical, stress rate in conjunction with the fatigue testing rate. However, because the stress rate in different fatigue tests must also be maintained constant, this calls for careful test design. For instance, test frequency adjustments will be necessary for any changes in R-ratios. Fatigue investigations that attempt to control stress rates instead of loading frequencies can be found in Thompson et al. [48], which is discussed in detail in Section 3.

2.3. Short-term strength in S–N curves

The need of inferring short-term strength from S–N curves arises when the original S–N curve was plotted on an absolute stress scale rather than a SL scale. This is particularly common in literature earlier than the 1960s. A few of them have listed the short-term strength, allowing a conversion from absolute stress to SL. In other cases, however, the short-term strength must be approximated as the intersection of S–N curves with the ordinate. Herein, the monotonic loading pattern in short-term strength tests is interpreted as half a loading cycle at 100% SL. This corresponds to an x coordinate of −0.3 on a log scale, which is roughly equivalent to the intersection value.

However, the accuracy of such extrapolation largely depends on the regression line provided by the original authors. This can be demonstrated in Fig. 1, where results of bending tests carried out by Kraemer [28] are replotted on a converted SL scale. Extrapolation of the original regression line is illustrated in black and suggests a value of

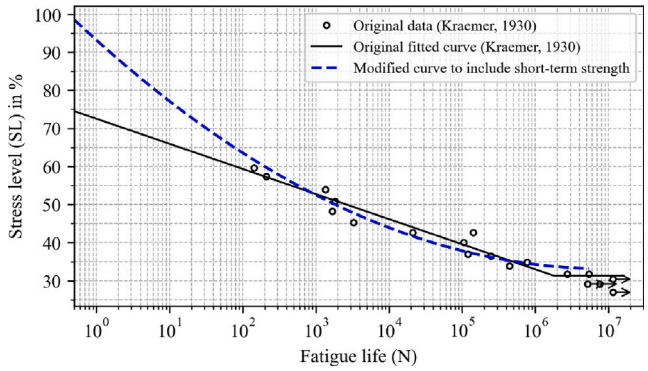


Fig. 1. Modified S–N curve of spruce subjected to bending fatigue load by including the short-term strength.
Source: Adapted from Kraemer [28].

approximately 75% of the recorded short-term strength. If one includes the actual short-term strength into the dataset, a regression curve asymptotic to a horizontal line indicated by the blue dashed line in Fig. 1 will be more reasonable.

2.4. Displacement control and load control

Different test control schemes are distinguished in fatigue tests and may influence the results. In load control, a constant load is applied periodically to the specimen, keeping both the load and SL consistent throughout the test. However, due to the viscoelastic properties of wood, displacement may increase over time. Conversely, in displacement control, the displacement is maintained constant, while the load and SL may fluctuate.

Plotting S–N curves typically requires a load-controlled test scheme. Since each data point is based on test conducted at a certain stress value. However, due to limitations in early testing apparatus, displa cement-controlled tests frequently occur in early literature on bending fatigue. Herein, two test apparatus need to be differentiated: a rotating bending machine that applies constant stress and alters the stress distribution by rotating the round-shaped specimens; and a flat-plate bending machine that restricts the maximum deflection within a load cycle [29].

If S–N curves are drawn in a displacement-controlled test based on the initially applied SL, one may expect an overall shift of the curve, with longer fatigue lives than those in a load-controlled setting with the same initial load. This shift may be negligible if the initial SL is within the elastic range. This is reflected in the bending moment drop of beech recorded by Kuech [30], as depicted in Fig. 2. The moment drop at a SL of around 36% is hardly visible even up to one million cycles, whereas for higher SL up to 65%, a gradual drop precedes the abrupt fatigue failure.

2.5. Criteria to stop fatigue tests

Selection of the criteria to determine the fatigue failure is another factor that may influence S–N curves. Herein, two categories can be characterized: the stress-based failure criterion and the strain-based failure criterion. Employing either criterion alone with insufficient threshold values may restrict the ability to adequately indicate specimen failure. With stress-based criteria, the drop of stress during the test is monitored and a test is considered complete when the stress is decreased by a certain percentage. Different percentage values were adopted in literature, ranging from 10% to 50% [10,51,52]. The extent to which this affects S–N curves certainly relies on the specific test conditions and specimen properties. As an example, the NOC for a moment drop of 10% and 50% did not deviate much considering the

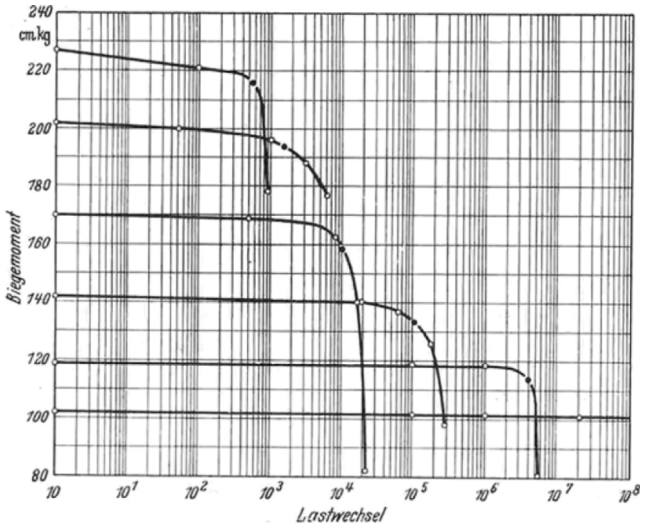


Fig. 2. Decrease of bending moment in a displacement-controlled fatigue test of beech LVL specimens (original graph captured from Küch [30]). The labels on the graph are in German. The *y*-axis is labeled "Biegemoment" (Bending Moment, in [cm kg]), and the *x*-axis is labeled "Lastwechsel" (Number of Cycles). The stress levels for each curve, estimated by the author, are 65%, 58%, 50%, 42%, 36% and 32%, in descending order from top to bottom.
© 1969 [Springer-Verlag], used with permission.

results shown in Fig. 2 obtained by Küch [30], at least not on a logarithmic scale. In all SL involved, the gradual moment decrease prior to the abrupt "failure stage" did not exceed 5%. However, for the ductile specimen tested by Kollmann [29], depicted in Fig. 3, the difference between fatigue life based on 10% and 50% moment drop was approximately 2.5×10^5 NOC, which is not a negligible magnitude even when plotted on a logarithmic scale (5 vs 5.54).

Strain-based criteria are mainly relevant for compression cases. Buckling is the predominant failure mechanism for compression and specimens may not lose all of their load bearing capacity after failure. In some literatures, a strain threshold is thus selected as test-stopping criteria. Herein, a difference between strain thresholds in short-term tests and fatigue tests generally exist, due to the delayed strain in fatigue tests. For instance, Ogawa et al. [47] used a strain value of 0.05 and 0.3 to signify the short-term "failure" and the fatigue "failure", respectively, using perpendicular-to-grain compressive tests. In this case, the applied SL for fatigue tests may even exceed 100%, since the short-term "failure" strain of 0.05 does not indicate the complete failure, and the specimen may survive some fatigue loading cycles before the delayed strain reaches 0.3. Therefore, direct comparison between fatigue tests with different criteria to stop the test may not be feasible.

Kommers [32] also applied a strain-based criterion for his displa cement-controlled cantilever bending tests. The mid-deflection of the cantilever beam increased with time despite the fixed deflection at the free end. A deflection increase of 0.076 mm was selected as test-stopping criterion, which is rather an indication of failure initiation, since the remaining strength of these tested specimens could still reach 85% of the original short-term strength. Also here, a shift of S–N curves to the left may be anticipated.

3. Comparison of S–N curves

An attempt is made in this work to compare S–N curves available in literature and to draw general conclusions on the influence of main fatigue parameters. Appendix gives a summary of literatures that contain experimental investigations on fatigue behavior of wood and

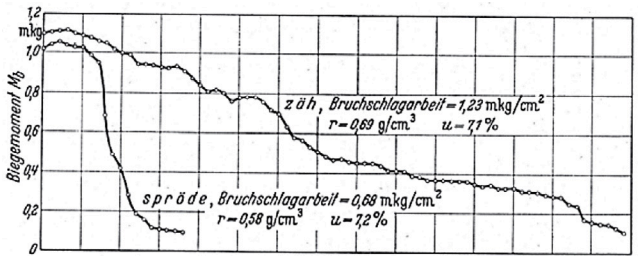


Fig. 3. Decrease of bending moment in a displacement-controlled fatigue test of ductile and brittle ash specimens (original graph captured from Kollmann [29]). The labels on the graph are in German. The *y*-axis is labeled "Biegemoment Mb" (Bending Moment, in [m kg]). The *x*-axis is unlabeled in the original literature. Based on the corresponding graph in [49], it is assumed to represent the number of cycles, spanning from 10^4 to $70 \cdot 10^4$ cycles. The left-hand line marked as "spröde" represents brittle behavior, while the right-hand line marked as "zäh" represents ductile behavior. "Bruchschlagarbeit" corresponds to fracture energy in [m kg/cm^2]. "r" and "u" denote the density and moisture content of the specimen, measured in [g/cm^3] and [%], respectively.
© 1941 [Julius Springer in Berlin], used with permission.

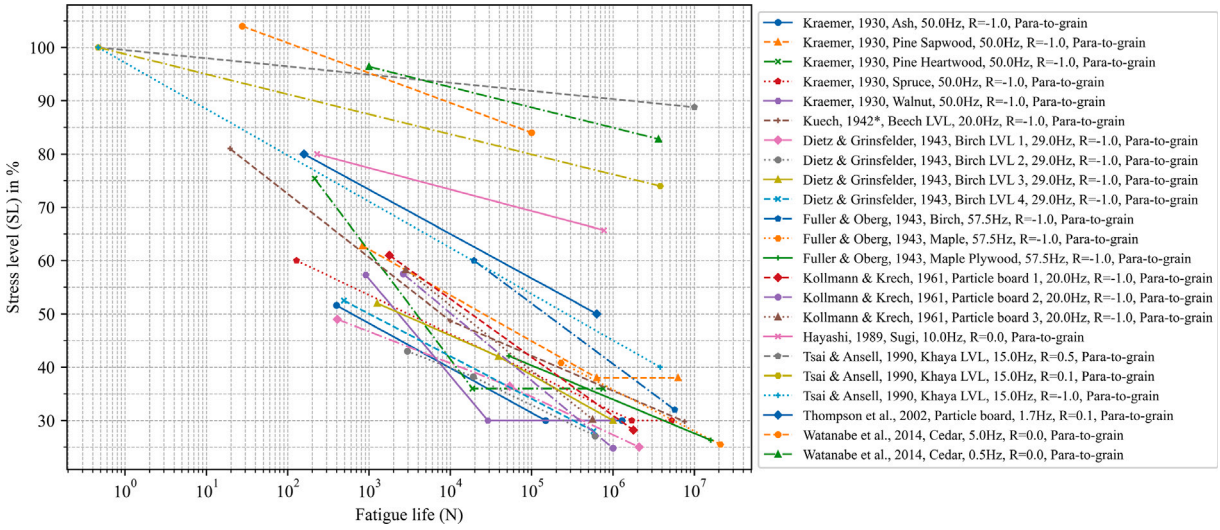


Fig. 4. Combined S–N curve for wood fatigue under Bending. *Küch [30] applied two different frequencies: 2 Hz for high stress levels and 20 Hz for low stress levels.

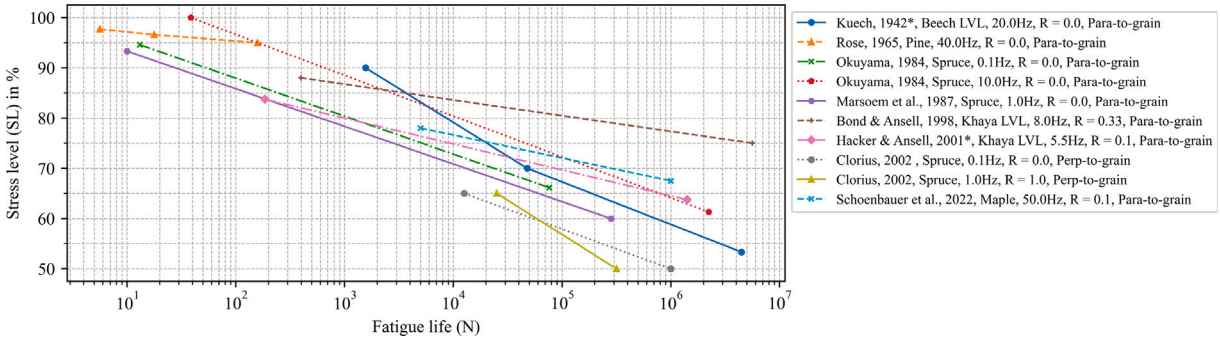


Fig. 5. Combined S–N curve for wood fatigue under Tension and reversed loading. *Küch [30] applied two different frequencies: 2 Hz for high stress levels and 20 Hz for low stress levels. *The frequency that Hacker & Ansell [50] applied ranges from 4 to 7 Hz.

wood products. A total of 101 items are listed regarding the loading pattern (SL, R ratio, frequency, waveform, NOC), the test condition (temperature, humidity level/moisture content), species and product types. For the reasons discussed in Section 2, special focus is given on whether the test has been performed displacement-controlled or load-controlled.

Despite the large number of experimental researches found, valid S–N curves that can be used for comparison are scarce. Nine literatures containing bending fatigue tests for wood and wood products are used to replot S–N curves in Fig. 4. Eight literatures are used for pure tension fatigue (see Fig. 5). Seven literatures contain compression-compression or tension-compression fatigue data are replotted in Fig. 6. The corresponding literature can be found in the figure legends. Main observations from comparing these S–N curves are discussed below.

To replot the S–N curves, data points are manually extracted from the published graphs in the referenced literature. As shown in Figs. 4, 5 and 6, two to three representative data points, which best capture the trend of the original fitted curves, are selected and displayed. To avoid the distraction of runouts, the part of curves that contains runouts is intentionally excluded. The inadequate information included in certain researches makes it challenging to identify the precise criteria that were applied to assess the reference short-term strength, The comparison that follows is based on the assumption that all sources use the mean

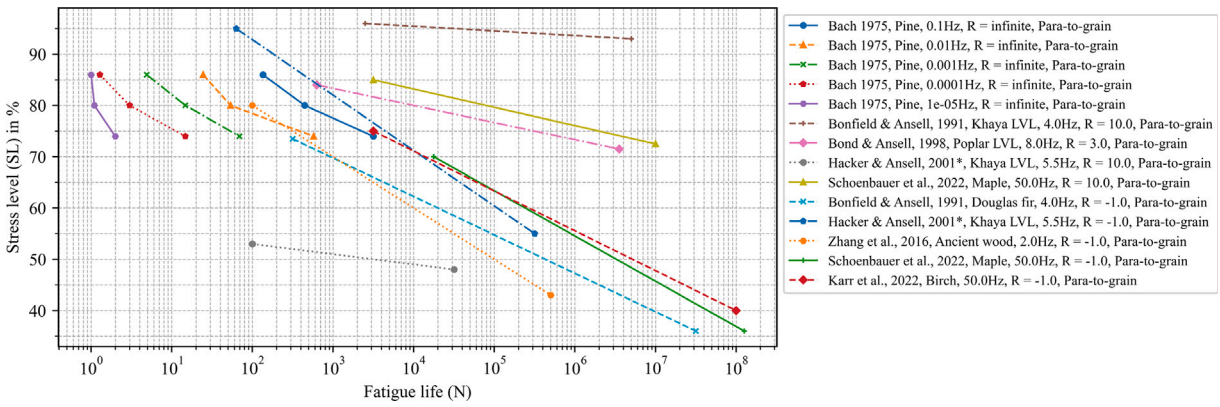


Fig. 6. Combined S–N curve for wood fatigue under Compression. *The frequency that Hacker & Ansell [50] applied ranges from 4 to 7 Hz.

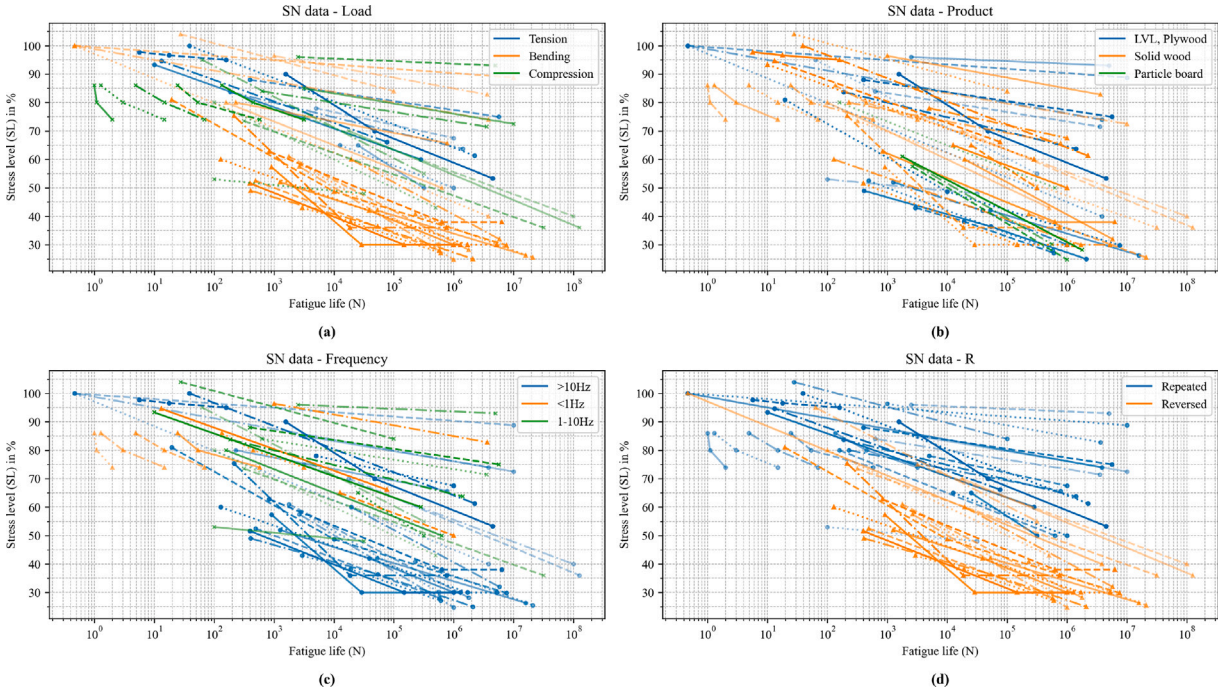


Fig. 7. Combined S–N curve for wood fatigue, color-coded by different factors: (a) Load type; (b) Wood product type; (c) Frequency; (d) R ratio.

strength measurements from standard testing that lasts between two and seven minutes.

3.1. Loading type

Fig. 7(a) illustrates the entire database, color-coded by different loading types. Bending fatigue has been the most widely investigated loading type, with its majority of S–N curves laying below the S–N curves from the uniaxial fatigue tests. This is mostly related to the frequent use of reversed loading in early bending studies. Fig. 8 excludes the reversed cases and tests with a frequency of lower than 1 Hz for a more focused comparison between tension, bending and compression. Most reported curves tend to converge at the short-term strength point (SL = 100%). However, the average slope from tensile fatigue tests seems to be higher than that from compression and bending, indicating that tension may be a less favorable case in terms of fatigue life.

If data from reversed fatigue tests are included (Fig. 7(a)), the lowest SL that leads to failure within 10 million NOC for bending is around 30%. This is consistent with the reported endurance limit of 22% to 36% for bending and tension, as discussed previously in Section 2. However, all replotted data from repeated fatigue tests (Fig. 8) suggest a higher

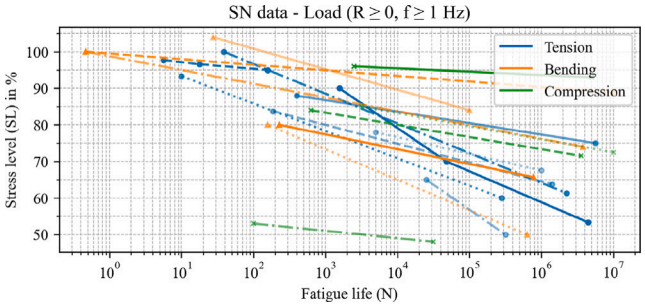


Fig. 8. Comparison of S–N curve for different loading types, limited to repeated cases.

SL for failure above 10 million NOC. Given the high degree of scatter in the data, it is difficult to draw a definitive conclusion about the exact value of endurance limit. However, it is clear that for repeated bending, tension, and compression, virtually no failure occurs within 10 million NOC at SL below 50%.

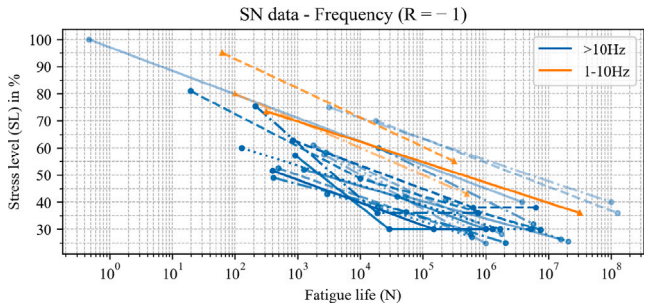


Fig. 9. Comparison of S–N curve at different frequencies, limited to reversed cases.

3.2. R ratio

One of the most clear conclusions that can be drawn from color-coding different parameters is regarding the *R* ratio. As depicted in Fig. 7(d), when the loading conditions are reversed, fatigue is significantly more severe compared to when loading is repeated. This trend is consistent, regardless of the wood species, loading types or the loading conditions. Fortunately, reversed loading in uniaxial direction is only possible at very low SL and is rare in practice. However, wooden beams and joints may experience reversed bending due to dynamic loads such as wind. Moreover, the gravity load of wind turbine blades are primarily under reversed bending. For those particular applications, special attention needs to be paid to fatigue design.

3.3. Frequency

The comparison of loading frequency is a complex topic that involves stress amplitude, loading rate and duration of load. If the stress amplitude is high, a higher loading rate is expected, potentially influencing the response of wood due to its viscoelastic nature. On the other hand, if the loading frequency is low enough, fatigue loading may be considered as equivalent to static loading. In that case, the accumulated duration of load instead of the NOC to failure needs to be plotted against SL as an indication of fatigue life. Bach [46] carried out pulsating fatigue tests (square wave) under compression and explored different frequencies ranging from 1×10^{-6} to 0.1 Hz. His results revealed a clear trend: at the same SL, specimens could resist a higher NOC to failure with increasing frequency and the duration of load theory applies well to this frequency range.

The influence of frequency cannot be derived clearly from the graph that has been presented in Fig. 7(c). Nevertheless, a clear trend of shorter fatigue life at higher frequency (> 10 Hz) can be observed when the data are limited to reversed fatigue, as shown in Fig. 9. For repeated loading, several literature has attempted to compare NOC to failure for various frequencies. Okuyama et al. [53] performed tensile fatigue tests on sitka spruce with a frequency of 10 Hz and 0.1 Hz. A clear shift of S–N curve to the right side was observed for 10 Hz group. For compression, Clorius compared the fatigue life at 1 Hz and 10 Hz for 80% SL. 10 Hz group showed a longer fatigue life for specimens conditioned at 85% humidity level but a shorter fatigue life for those conditioned at 65%. For bending, Sasaki et al. [54] applied both square wave and triangular wave on Japanese cedar. It was also concluded that the lower frequency of 0.5 Hz led to shorter fatigue life compared to 2 or 5 Hz. However, opposite conclusion was drawn by Watanabe et al. [55], who found that lower frequency (0.5 Hz) resulted in longer fatigue life for hardwood species Selangan batu, compared to 5 Hz. This trend was only observed for lower SL, possibly implying a stronger influence of frequency with increasing SL.

As explained previously, a potential effect of comparing different frequencies is that the loading rate may vary with different SL. Thompson et al. [48] compared the repeated bending fatigue properties of particle boards by fixing a low, medium and high stress rate (1.2 MPa/s, 12 MPa/s and 150 MPa/s). Three frequency ranges were obtained accordingly: 0.015–0.15 Hz, 0.15–3.0 Hz and 3.0–15.0 Hz. Their results indicated a decreasing fatigue life for lower frequency range.

3.4. Waveform

The shape of the waveform also affects the fatigue behavior of wood. Although comparison based on collected S–N curves could not be achieved due to data insufficiency, the effect has been highlighted by studies that compared the strain energy work density under different waveforms (see Marsoem et al. [56] and Gong & Smith [57]). Through low-cycle fatigue tests, Gong & Smith revealed that in compressive fatigue, the damage accumulates more rapidly under square waveforms, with twice the work density resulted from a comparable triangular or sinusoidal shape. For comparison between sinusoidal form and triangular form, it was observed that the number of specimens that failed within 150 NOC at a SL of 90% was higher under sinusoidal form. The experimental investigation by Marsoem et al. [56] on tension supported these findings by comparing both fatigue lives and the energy density loss during fatigue loading. An explanation was given by comparing the duration of maximum load and the rate of loading – the square wave has the highest duration of maximum load, whereas the sinusoidal wave has a higher value of maximum loading rate than triangular wave, despite the same duration of maximum load at the latter two.

3.5. Wood and wood products

Tsai & Ansell [3] concluded that laminated wood (Plywood and LVL) does not differ essentially from solid wood in bending fatigue. This is reinforced by the combined S–N curves illustrated in Fig. 7(b). The reported tests on laminated wood, which primarily focused on bending fatigue, reveal no significant differences in the slope or range of the S–N curves from that of solid wood. Dietz and Grinsfelder [31] analyzed the stress distribution of Plywood and LVL and monitored the failure process of both under cantilever bending fatigue. They found that although the bending stress may distribute differently in Plywood and LVL, the fatigue failure of both cases largely depends on the outermost ply, which is essentially the same as solid wood. The change of shear stress distribution in certain Plywood configurations has potentially negligible effect on the failure initiation, since the governing design requirement of laminated wood is hardly ever in shear. Fatigue experiments have confirmed that the bending damage initiated at the outermost wood layer rather than the glue line, regardless of the type of laminated wood [31]. For Glulam (Glue-laminated-timber), Sterr [58] also concluded that the investigated four adhesives does not have an influence on fatigue failure pattern.

The same S–N data from Fig. 7(b) are replotted in Fig. 10, with a distinction made between reversed bending and repeated bending. Similarly, laminated wood cannot be distinguished from solid wood. However, particle boards seem to exhibit different behaviors at reversed and repeated loading. For reversed loading, particle boards align with solid wood or laminated wood. Whereas in repeated loading, particle boards show a much lower fatigue resistance than the other two. Kollmann and Krech [51] commented that due to the high percentage of resin, particle board behaves more brittle compared to solid wood. Ansell [4] compared the hysteresis loops of OSB (Oriented Strand Board) and particle board at the same SL. It was found that particle board exhibits significantly higher residual strain, which was explained as the highly diffuse microstructural damages caused by its inhomogeneous and unconsolidated structure.

4. Stress–strain relationship during fatigue loading

Constitutive law is key to structural analysis of wood. Analyzing the stress–strain relationship of wood during fatigue loading is essential for establishing effective and reliable constitutive models. The following highlights main conclusions regarding different strain components and stiffness retardation during fatigue loading.

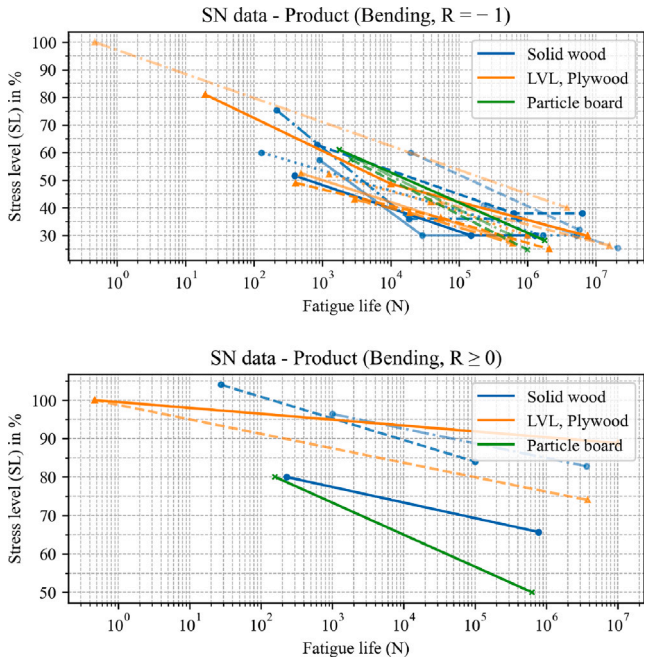


Fig. 10. Comparison of S–N curve for different wood products, differentiating reversed bending and repeated bending.

4.1. Viscoelasticity

It has been long established that wood exhibits "delayed" strain increase under sustained stress (creep), and shows stress recovery under sustained strain (relaxation). Both of the aforementioned phenomena can be attributed to the viscoelasticity of wood. Also, in fatigue of wood, the occurrence of delayed strain has been recognized [59,60]. In this work, two delayed strain components are distinguished: the recoverable part, which is referred to as viscoelastic strain; and the irrecoverable part, denoted as viscous strain (also referred to as "plastic strain" in some literature).

The existence of both viscoelastic and viscous fatigue deformation has been observed by Gillwald [38] through an intermittent bending test with displacement-controlled scheme. His results highlighted two distinct stress behaviors observed on beech LVL specimens: "$\Delta\sigma_{\text{recovery}}$" and "$\Delta\sigma_{\text{reduction}}$". The former indicates recoverable viscoelasticity, since the first load cycle after 15-hour interval always required a higher stress to reach the same deflection. While the latter suggests irrecoverable deformation, because the overall stress to reach the same deflection throughout the fatigue test clearly decreased.

Similar behaviors are observed in a load-controlled intermittent fatigue test by the author. European ash specimens are prepared and subjected to compressive fatigue loading in parallel-to-grain direction. A relatively high SL of 78% is used and the loading frequency is 1 Hz. Each loading interval consists of 400 fatigue loading cycles and a recovery phase of 10 minutes. Fig. 11 illustrates the fatigue strain at each cycle and residual strain during the recovery phase, both normalized by fatigue strain at the first loading cycle. The strain increase, denoted as "$\Delta\varepsilon_{\text{increase}}$", represents the sum of viscoelastic and viscous strain. At the end of each recovery phase, a certain percentage (exemplified by "$\Delta\varepsilon_{\text{recovery}}$" in Fig. 11) can be recovered, representing the contribution of viscoelastic strain. In contrast, the gradual increase of the remaining irrecoverable strain with each successive interval clearly demonstrates the development of viscous strain.

Bach [46] attempted to map out different strain components quantitatively using low-cycle compressive fatigue tests with relatively high SL of 74%, 80% and 86%. Strain components were plotted on a relative scale to the initial strain at each corresponding SL. It was concluded that a lower SL led to higher relative viscosity but a consistent level of recoverable viscoelasticity. The observed viscous strain was of a magnitude of two to three times the viscoelastic strain. However, it is worth highlighting that Bach applied a one-to-one sample matching technique for determining the reference short-term strength. Moreover, Bach did not conduct strain recovery tests on a single specimen to obtain the development of strain components with time. Instead, he simply assumed identical fatigue lives for a group of specimens and combined tests results of specimens that were unloaded at various time intervals. The test results might not be wholly convincing taking into account the large scattering nature of wood specimens.

4.2. Residual strain

Residual strain can be considered as the sum of viscoelastic and viscous strain. Analyzing residual strains, particularly in increasing-amplitude fatigue tests, provides insights into how the same specimen responds differently to various SL. Myslicki et al. [62] observed a turning stress that potentially signifies microscopic damage initiation in increasing-amplitude fatigue tests. Uniaxial reversed fatigue tests were performed on beech specimens, where the strain value at complete unloading of each cycle was recorded. The residual strain (originally referred to as "plastic strain") exhibits nearly linear growth at lower stress values, but changes to an exponential growth at higher maximum stress values. Based on the transition, Myslicki et al. [62] identified a turning stress of 25 MPa. Subsequent constant-amplitude fatigue tests implementing this turning stress suggested neglectable residual strain up to a million NOC. It was therefore inferred that this turning stress corresponds to the endurance limit of the material.

Launay et al. [63] carried out tensile tests subjected to complex loading on short-glass-fiber reinforced polyamides. An important observation was that the irreversible viscous strain appears above a certain stress threshold. Potentially, the turning stress, obtained by Myslicki et al. [62], may be utilized to help determine a similar stress threshold for fatigue loading of wood. However, this determination is based on the residual strain at complete unloading, which is feasible only under reversed fatigue loading. The author attempts to investigate whether the minimum strain (ε_{min}) observed in each loading cycle can be utilized to identify this turning point for repeated fatigue tests. European ash specimens are tested with a loading frequency of 1 Hz. The preliminary results are shown in Fig. 12. If σ_{min} is kept constant in the increasing-amplitude test, ε_{min} theoretically represents the sum of the residual strain and a constant elastic contribution corresponding to σ_{min}. As shown in Fig. 12, the turning point determined by ε_{min} reaches 30 MPa, which corresponds to 66% of the average short-term compressive strength. A direct comparison with the results by Myslicki et al. [62] is difficult since they did not report the compressive strength of the tested material. Nevertheless, it can be observed that the exponential growth of strain after the turning point in Myslicki et al. [62] is significantly more pronounced than that shown in Fig. 12. Given that Myslicki et al. applied 10^4 NOC for each stress value, whereas the author applies only 200 NOC, it can be concluded that the determination of turning stress is highly dependent on the number of applied loading cycles.

4.3. Residual stiffness

Monitoring the change of residual stiffness during fatigue loading is an effective approach to acquire whether gradual deterioration of material exists. Various methods and techniques have been employed to derive the residual stiffness from the stress–strain relationship, as depicted in Fig. 13. Gong et al. [61] derived the residual stiffness E_N using Eq. (1):

$$E_N = (\sigma^N_{\text{Max}} - \sigma^N_{\text{Min}})/(\varepsilon^N_{\text{Max}} - \varepsilon^N_{\text{Min}}) \quad (1)$$

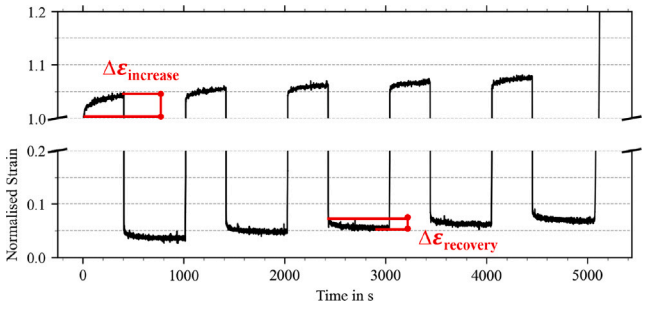


Fig. 11. Strain–time relationship of European ash specimens subjected to intermittent compressive fatigue loading, with strain normalized by the maximum strain at the first loading cycle.

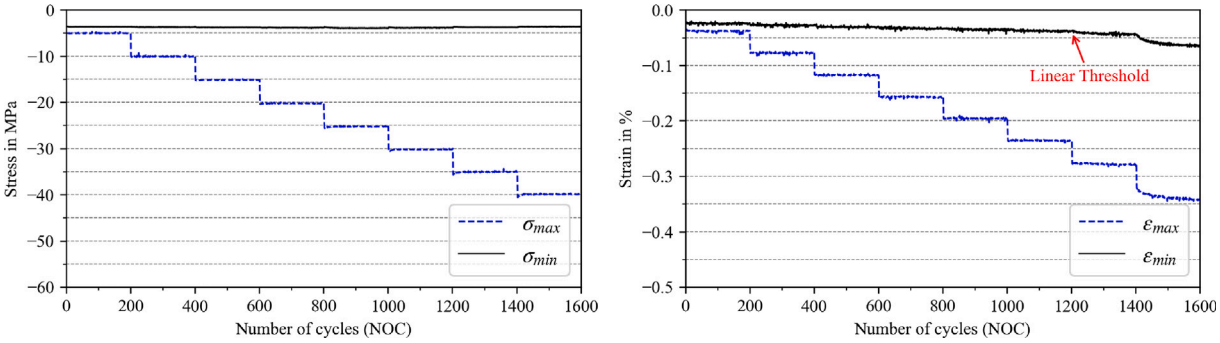


Fig. 12. Cyclic strain development determined in an increasing-amplitude compressive fatigue test on European ash, with a frequency of 1 Hz.

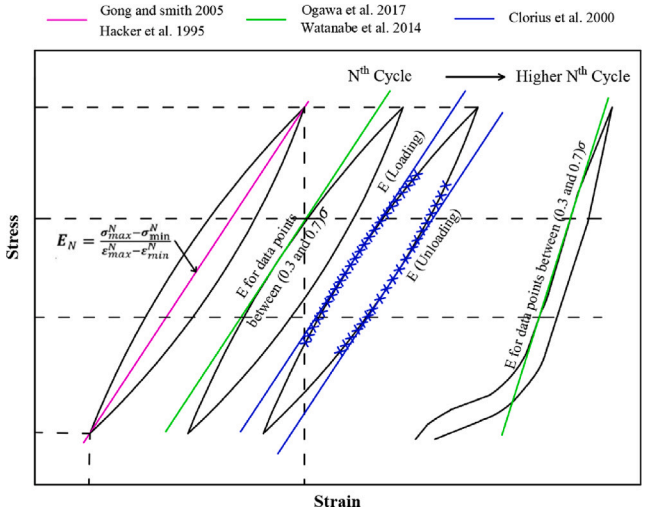


Fig. 13. Different definitions of residual stiffness.

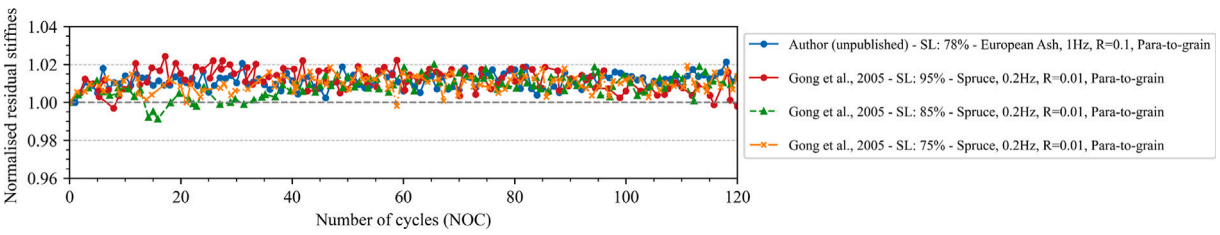


Fig. 14. Residual stiffness change recorded during shorter-period compressive fatigue tests, combining data from Gong et al. [61] and test results by the author. Normalized by the initial stiffness.

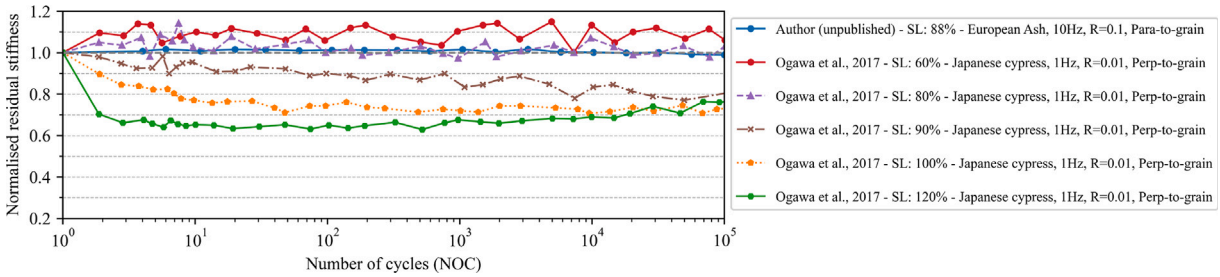


Fig. 15. Residual stiffness change recorded during longer-period compressive fatigue tests, combining data from Ogawa et al. [47] and test results by the author. Normalized by the initial stiffness.

Where, σ^N_{Max} and σ^N_{Min} represent the highest and lowest stress at each loading cycle, respectively. $\varepsilon^N_{\text{Max}}$ and $\varepsilon^N_{\text{Min}}$ are the highest and lowest strain at each loading cycle, respectively. This approach, while being the most practical way, may not correctly represent the stiffness of the material since it contains possible nonlinearity at extremely low and high stresses.

In other cases, the residual stiffness was distinguished between loading and unloading phases, typically following the linear slope of the middle part of the stress–strain curve. Ogawa et al. [47] and Watanabe et al. [55] focused on the loading phase, calculating stiffness based on the slope between $0.3\sigma^N_{\text{Max}}$ and $0.7\sigma^N_{\text{Max}}$. Clorius et al. [43] determined residual stiffness for both loading and unloading phases. The determination was restricted to the interval with specified loading rate, where two adjacent datapoints show a stress difference of more than 0.4 kN.

Different conclusions have been drawn regarding residual stiffness changes during fatigue loading before failure. From a series of low-cycle compression fatigue tests on spruce, Gong et al. [61] concluded that no remarkable changes in E_N could be detected over the first 120 cycles. A relatively low frequency of 0.2 Hz was applied and the SL varied from 75% to 95%. This conclusion is confirmed by the author with tests on European ash with a higher frequency of 1 Hz and a SL of 78%, as depicted in Fig. 14. All stiffness values are normalized by the initial stiffness value. For a consistent comparison, the author chooses to calculate the residual stiffness according to Eq. (1). The normalized stiffness across all groups, irrespective of species and SL, exhibits a slight increase and fluctuates between 1 and 1.02.

A much more pronounced residual stiffness fluctuation was reported by Ogawa et al. [47], who investigated the compressive fatigue behavior of Japanese cypress LVL in long-term fatigue tests. Notably, the tests were performed in perpendicular-to-grain direction, with stiffness change recorded up to 0.8 million NOC. The reference short-term strength value was obtained through correlation with density values. As depicted in Fig. 15, for lower SL up to 80%, a "strengthening" effect was observed, possibly due to the "densification" caused by compressive stress in the radial direction. The normalized residual stiffness based on the initial stiffness experiences a rapid change during the first load cycles, but oscillates within a rather small range up to one million NOC. For higher SL except 120%, the stiffness decreased over the cyclic loading. In general, the normalized value obtained by Ogawa et al. [47] showed a clear negative correlation to the applied SL. Fig. 15 also presents the stiffness change observed by the author in long-term tests conducted at a higher frequency of 10 Hz. European ash specimens are subjected to compressive loading in parallel-to-grain direction, with a SL of 88%. The residual stiffness is calculated according to Eq. (1), which exhibits a similar fluctuation range as that observed in Fig. 14. The normalized stiffness shows a slight initial increase, followed by a drop after 10^4 NOC.

In another attempt by Gong [64], where the residual stiffness was monitored until fatigue failure, a consistent trend of decrease was observed in residual stiffness. Sample matching was applied to determine the applied stress for two SL - 85% and 95%. Compressive fatigue tests were performed in parallel-to-grain direction. Regardless of the difference in loading and unloading phase, a clear stiffness reduction was obtained, which was gradual at the beginning, followed by an abrupt drop near fatigue failure. The distinct residual stiffness drop in this case can be a result of Gong's definition of residual stiffness, which simply takes the highest and lowest point for calculation. As illustrated in Fig. 13, according to Hacker [65], the shape of hysteresis loop changes gradually from elliptical curves (to the left side of the graph) to S-shaped curves (to the right side of the graph). Gong's calculation may result in lower stiffness values at high NOC compared to other researches.

The abovementioned researches are restricted to stiffness monitoring in repeated compressive fatigue tests ($R > 1$). Hacker [65] conducted an extensive study on residual stiffness changes for axially-loaded specimens. Particularly the behavior under different R ratios was compared and discussed. The results suggested a consistent gradual drop of residual stiffness for reversed loading cases. In contrast, the pure tension case exhibited more or less a stepwise decrease, which, according to Hacker [65], is potentially attributed to initiation and propagation of cracks. For the pure compression case, a rather irregular change was obtained.

5. Fatigue life modeling

The majority of existing wood fatigue models predict fatigue life based on phenomenological observations and do not take into account the physical damage mechanism. In this work, fatigue life models are classified into two categories based on their fatigue criteria:

- Theoretical models that use a time-to-failure criterion, including S–N curves, constant life diagrams and duration-of-load (DOL) models.
- Progressive damage models that propose an evolution law based on stress–strain behaviors, taking advantage of either the degradation of residual stiffness, or the dissipated energy.

Models that implement fracture mechanics theory are excluded, since notched specimens are mostly involved and stress concentration takes place, which is out of the scope of this analysis.

The symbols and notations that were used by the original researchers are preserved to avoid ambiguity.

5.1. Constant life diagram

The S–N curve has been extensively discussed in Sections 2 and 3. A clear drawback is that S–N curves alone do not provide information on the effect of different R ratios. The constant life diagram is a further development that helps predict fatigue lives under loading conditions for which no experimental data exist. Fatigue life data from tests with different R ratios are plotted in $\sigma_a - \sigma_m$ plane, with the points corresponding to the same expected fatigue life connected to a curve, as illustrated in Fig. 16.

The linear triangular shape shown in Fig. 16 is a widely-used constant life diagram in composites. It can be conveniently derived by

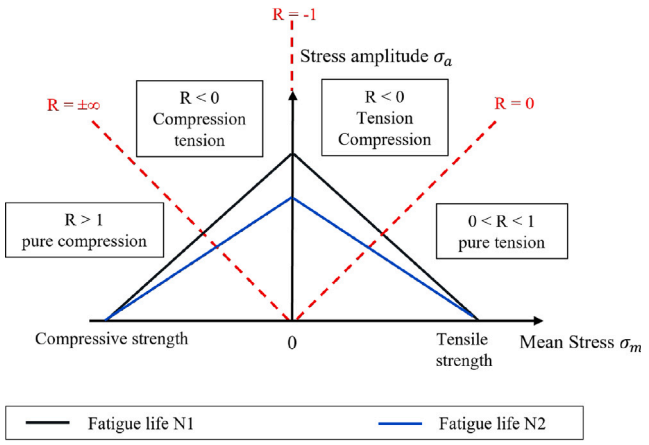


Fig. 16. Illustration of a linear constant life diagram.

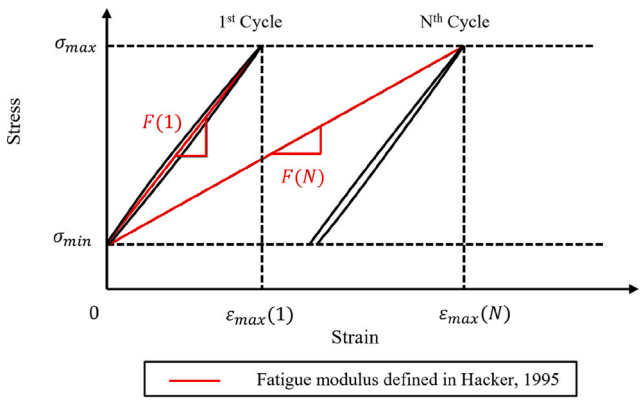


Fig. 17. Definition of fatigue modulus.

connecting the short-term strength σ_u and fatigue strength σ_e at R = −1. Eq. (2) shows the mathematical form of the linear constant life diagram. Bond & Ansell [66] attempted to draw the linear constant life diagrams for axially loaded LVL specimens from Khaya and Poplar. However, fatigue tests suggested rather irregular shape of constant life diagrams. It was concluded that the linear triangle constant life diagram is a conservative estimation of the fatigue performance.

$$\sigma_a = \sigma_e(1 - \sigma_m/\sigma_u) \tag{2}$$

5.2. Duration of load model

The DOL models (Gerhards [67], Barrett and Foschi 1978 [68], or Yao and Foschi [69]) are relatively simple in form and have been widely used in creep life modeling of wood. Although they were originally obtained from experimental observations, van der Put [70] has proven that they can be derived on the basis of the reaction kinetics theory proposed by Krausz and Eyring [71].

The DOL approach in fatigue context is essentially an extrapolation of creep modeling to fatigue modeling. It considers the accumulated duration of maximum load during cyclic loading and correlates fatigue loading with a creep loading of the same load duration. Van de Kuilen [6] analyzed the compressive fatigue test results obtained by Bach [46] and concluded that fatigue loading with a frequency of 0.1 Hz and less can be treated as static loading. The fatigue lives of tests at 10^{-6} to 10^{-1} Hz plotted on an accumulated-time scale appeared to be coincidental. Clorius [43] applied higher range of frequencies up to 10 Hz and found the DOL approach alone to be invalid for these cases. It was concluded that a combined approach integrating both S–N curves and DOL may be more appropriate for higher range of frequencies.

An attempt has been made by Kohara & Okuyama [72] to link NOC to failure and DOL based on a modified Miner's rule. As depicted in Eq. (3), four model parameters are required: a creep life T_{crp}, a reference fatigue life N_{ftg}, and two model constants a and b. Failure is determined whenever the summation of two terms reaches unity: one related to the accumulated duration of fatigue loading, and the other related to the NOC. Bending fatigue tests with a frequency of 0.1 Hz suggested a value of 1 for the constant a, and a value of 0.02–0.5 for the constant b, respectively. Later, Gong [8] also validated this model using compressive fatigue tests with a frequency of 0.5 Hz.

$$1 = (T/T_{\mathrm{crp}})^a + (N/N_{\mathrm{ftg}})^b \tag{3}$$

However, the distinct magnitude difference between parameters a and b obtained by both Kohara & Okuyama [72] and Gong [8] suggests a much higher contribution of DOL over NOC using this model. This differs from the observation made by Bach [46] and Clorius [43], who inferred a dominant effect of DOL at lower frequencies.

Moreover, a notable limitation of the model by Kohara & Okuyama [72] appears when applying such model to the selected reference fatigue test. Regardless of the selection, the model consistently predicts a shorter fatigue life for the reference fatigue test compared to the actual test result, since the second term alone in Eq. (3) already equals unity at the actual failure.

5.3. Residual stiffness model

Gong [8] described the correlation of residual stiffness degradation to NOC to failure for low-cycle repeated compression tests through Eq. (4). The residual stiffness is taken as the stiffness monitored at each fatigue loading phase. The damage variable D can be experimentally obtained using $D = 1 - E_r/E_0$, where E_r denotes the residual stiffness, and E_0 indicates the stiffness at the first cycle. By monitoring the change of residual stiffness for a certain number of cycles, α and β can be fitted, allowing subsequent prediction of the fatigue life N_f. Fatigue failure is considered to be reached when $D = 1$. The effect of fatigue parameters, including SL, R ratios and waveforms, are reflected in the model parameter α and β.

$$D = 1 - (1 - \alpha)(1 - \frac{N - 1}{N_f - 1})^{\beta} \tag{4}$$

The intention of the proposed residual stiffness model is probably to predict fatigue life by monitoring a shorter period of fatigue tests. However, Gong's test results with SL of 85% and 95% showed only slight increase of D (less than 0.05) over half of the fatigue life, which will be difficult to detect given the highly sensitive measurement of residual stiffness even with the most advanced techniques available. Moreover, an essential assumption here is that a continuous decrease in residual stiffness will occur over the fatigue loading. This could not be established for all SL, neither with low-cycle fatigue tests conducted by Gong [61], nor with high-cycle fatigue tests by Ogawa et al. [47], as discussed previously in Section 4.

A different approach based on the degradation of fatigue modulus was proposed by Hacker [65]. As depicted in Fig. 17, the two red lines illustrate the definition of fatigue modulus F at the first and the Nth cycle, respectively. Rather than taking the slope of the applied stress versus the strain increment within each loading cycle, Hacker [65] considered the slope of the applied stress versus the maximum accumulated strain at each load cycle. As shown in Eq. (5), the correlation between NOC to failure and fatigue modulus F was established for high-cycle compression and tension fatigue tests, in both repeated and reversed settings. Parameters α and β are model parameters fitted for different loading conditions. Compared to the residual stiffness, fatigue modulus incorporates the effect of previously accumulated linear and non-linear viscoelastic strain. Consequently, a larger range of variation can be observed than that in the residual stiffness. For the conducted

compressive fatigue tests, the fatigue modulus approach appeared to be promising, whereas tensile fatigue tests appeared to be more brittle and showed insufficient gradual decrease in fatigue modulus for fatigue life prediction.

$$log N_f = \alpha - \beta \cdot log|F| \tag{5}$$

5.4. Energy dissipation model

The area of the hysteresis loop in a stress–strain plot implies the dissipated energy density within a full load cycle. Kohara & Okuyama [73] found a strong correlation between the NOC to failure N_f and the nonlinear component of dissipated energy density H_b in tensile fatigue tests. The derived function is illustrated in Eq. (6). Model constants α and C can be estimated from experimental data. H_b represents the nonlinear contribution of dissipated energy density obtained in a single loading cycle. Empirical findings [40,56,73,74] have suggested that H_b is a constant value dependent on the combination of SL, waveforms, and wood species. As a result, the fatigue life of the corresponding loading conditions can be calculated using Eq. (6) once H_b is obtained.

$$H_b \cdot N_f^a = C \tag{6}$$

The partitioning scheme of dissipated energy density suggested by Kohara & Okuyama [73] follows Eq. (7). The total dissipated energy H_c within one cycle is divided into a linear term H_a and a nonlinear term H_b. σ denotes the maximum stress within a load cycle. The postulated stress threshold σ_0 was found to be consistently 37% of the short-term strength for six tested species. K_a, K_b and n are model constants that potentially depend on fatigue loading conditions and wood species. For model parameter K_a, an inverse proportional relationship to the Young's moduli of the material was also observed.

$$\begin{aligned} H_c &= H_a + H_b \\ H_a &= K_a \cdot \sigma^2 \\ H_b &= K_b \cdot (\sigma - \sigma_0)^n \end{aligned} \tag{7}$$

Watanabe et al. [55] developed a fatigue life model for specimens subjected to bending based on the total dissipated energy density accumulated at failure. The mathematical form of the model is illustrated in Eq. (8), where the total dissipated energy density is denoted as V_{acf} (originally referred to as "cumulative strain energy at failure"). A strong correlation was found between V_{acf} and the NOC to failure, regardless of SL and loading frequencies. Two species were tested and their total energy density dissipation were found to harmonize when normalized by the static strain energy V_{static}. Herein, V_{static} represents the bounded area by the stress–strain curve and the horizontal axis up to the maximum load in a static test.

$$V_{\text{acf}}/V_{\text{static}} = 0.654 N_f^{0.942} \tag{8}$$

Although validation of the proposed energy density dissipation model is not available for compression cases, an attempt is made by the author to implement the Watanabe model on energy density dissipation data obtained by Clorius et al. [43]. By taking the log of both sides, one easily converts Eq. (8) to a linear relationship between $log V_{\text{acf}}$ and $log N_f$ shown in Eq. (9). According to Watanabe et al. [55], model parameters α and β are independent of loading frequencies. Thus, test data with the same relative humidity level but different frequencies are combined and plotted in a $log N_f - log V_{\text{acf}}$ space. As depicted in Fig. 18, the data of both groups seems to exhibit a linear correlation, possibly fitting the Watanabe model. Notably, the fitted parameter α reaches 0.7 and 1.222 for the tested spruce specimens at low and high humidity levels, respectively, differing from the predicted value of 0.942 for both Japanese cedar and Selangan batu reported in Watanabe et al. [55]. Further tests are required to determine whether this discrepancy arises from differences between bending and compression tests or is simply a result of species-related characteristics.

$$log V_{\text{acf}} = \alpha \cdot log N_f + \beta \tag{9}$$

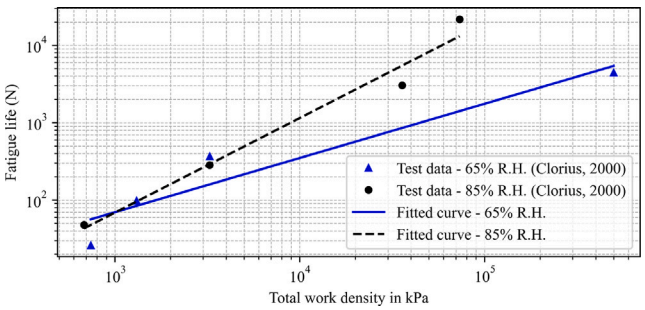


Fig. 18. Compressive fatigue test data by Clorius [43] fitted to the energy dissipation model proposed by Watanabe et al. [55].

6. Fracture morphology and failure mechanism

The physical observation of failure and fracture of wood under mechanical loading is crucial for achieving a thorough understanding of wood strength. Microscopy applications such as optical microscopy, scanning electron microscopy (SEM) and transmission electron microscopy, are instrumental in establishing the relation between wood structure and the initiation of fatigue failure. The following section differentiates between bending and uniaxial loading cases and provides an overview about both macroscopic and microscopic investigations into fatigue failure of wood.

6.1. Bending

Early researches on fatigue damage of wood focused on reversed fatigue subjected to bending. For such cases, Kraemer [28] proposed that fatigue damage primarily originates from fiber buckling due to compressive stresses. Kraemer's theory was based on the fact that the compressive strength of wood along its fiber orientation is significantly lower than its tensile strength. As a result, fiber buckling takes place prior to any tensile failure. During the cyclic loading phase where wood is subjected to tensile stresses, stress concentrations develop as a consequence of the fiber buckling. Over time, the unaffected fibers near buckled fibers gradually deteriorate and eventually break. Kohara et al. [75] studied the fatigue damage of beams under repeated loading and compared it with the damage under sustained loading. At both cases, a compressive buckling zone was observed. However, cracks occurred along the fatigue buckling zone, implying that there might be stress redistribution under the repeated cyclic loading, eventually leading to tensile stresses around the buckling zone.

Microscopic observations of fiber buckling during repeated fatigue tests were reported by Tsai & Ansell [3]. For a repeated cyclic loading scheme, the neutral axis of the specimen should be subjected to a minimal SL. Nevertheless, the development of compression folds towards the center of the specimen was clearly demonstrated, indicating the shift of the neutral axis towards the tensile side due to the accumulation of fiber buckling at the compressive zone. Sasaki et al. [54] explored the extent of neutral axis shifting in correlation with various stress peak levels. A noticeable increase in the thickness of the compressive layer at the failed surface was observed as the applied SL increased. Using a similar experimental configuration, Watanabe et al. [55] performed repeated bending tests on different wood species, subjected to different loading frequencies. They reported that more cracks on the compressive side were visible for the specimens that experienced longer fatigue lives, regardless of the implemented frequencies or wood species. Therefore, two distinct failure patterns potentially exist in repeated fatigue bending tests: A ductile pattern at low SL, where minor cracks were generated by excessive tensile stresses but remained relatively insignificant until the number of cracks reached a critical threshold; A brittle fracture pattern at high SL, where even a few cracks were sufficient to trigger immediate material failure.

6.2. Uniaxial loading

The fatigue failure mechanism of softwood in compression parallel to grain was investigated by Gong & Smith [8,64]. They studied the low cycle fatigue behavior of spruce and compared it to creep behavior, utilizing two types of microscopy. To understand the surface damage, they used "dark-field" light microscopy, while microtoming techniques were employed to understand damage initiation and development inside the material. According to their findings, the accumulation of damage resulting from creep and fatigue showed distinct characteristics. In creep tests, damage started and propagated from pre-existing kinks formed during the initial loading phase. In contrast, in fatigue tests, damage raised from both pre-existing kinks formed during the first load cycle and newly formed kinks induced by cyclic loading. The quantification of kinks demonstrated a robust correlation with relative cyclic creep and relative creep, establishing it as a pertinent and direct indicator of damage. Additionally, a similarity was found between the relationship of the number of kinks to time to failure and the relative deformation to time to failure for both creep and fatigue cases.

Regarding the influence of SL, the failure pattern could not be distinguished between higher and lower SL for pure compression cases, as reported by Okuyama, et al. [53], following a repeated fatigue test. In one specimen, a buckling line was observed after about 10^3 cycles of repeated loading at 90% of the static strength. Nevertheless, the specimen did not fail even after over 10^6 load cycles.

Rose [41] conducted repeated tensile and compressive fatigue tests at a frequency of approximately 40 Hz. After 3.5 million load cycles, unfailed specimens were tested with static loading to assess their residual strength. The results of the compression tests showed a statistically strong negative correlation between the remaining strength and the applied fatigue peak stress. In contrast, for the tension scenario, no substantial reduction in the remaining strength was observed with increasing fatigue peak stress. It was proposed that compressive stresses parallel to fiber prompted the lateral bending of the fiber, leading to localized loosening at the middle lamella. Whereas the alternating tensile stresses brought about a "stabilization" effect, reorientating the microfibril bundles in the cell wall to a higher degree of crystallization, eventually compensating the strength reduction caused by the microstructural loosening.

Curtu et al. [76] investigated the compressive fatigue of ash in different fiber directions for a very low loading frequency. A five-minute constant loading at a level below the static yield stress of ash was applied, followed by a two-minute unloaded break. Microstructural loosening of cell walls was observed. Notably, approximately 85% of the observed loosening was concentrated at the same locations as the rays. It was believed that the rays promoted the sliding of fiber bundles. The study also addressed the size effect on the compressive fatigue of ash wood. Similar to static tests, larger specimens tested parallel to the fiber direction exhibited significantly greater deformation in the fatigue tests. This was attributed to the higher likelihood of inherent defects in larger samples. In analogy to the effect of rays, these inherent defects facilitated the loosening at the middle lamella. Conversely, specimens that were compressed perpendicular to the grain showed a negative correlation between deformation and specimen size. In these instances, the wood fibers did not slide, but instead converged at positions with defects, resulting in a "strengthening" effect.

7. Conclusion and outlook

Bridge and wind turbine components made out of wood have been traditional applications where fatigue is the governing loading. With wood gaining renewed attention for innovative engineering applications, understanding its fatigue resistance has become increasingly important.

This paper analyses the current status of experimental investigations on fatigue of wood. Extensive data have been reported on fatigue of wood and wood products, essentially subjected to bending and tension. S–N curves have been focus of these investigations, which are believed to be practical indication of fatigue resistance. However, direct comparison of S–N curves between various researches can be difficult and inconclusive, due to the often different failure criteria and test setups. The most obvious conclusion drawn from comparing S–N curves is regarding the R-ratio – reversed loading tends to be the least favorable situation. Tension fatigue seems to show a less favorable situation, compared to compression and bending. Moreover, laminated wood products (LVL and Plywood) and particle boards produce essentially similar S–N curves as solid wood.

The stress–strain relationship is another important aspect in investigating wood under cyclic loading. Measurement of residual strain and its recovery reveals the presence of recoverable and irrecoverable strain components that are delayed, which can be attributed to wood's viscoelastic nature. Several attempts have been made to monitor the residual stiffness change during uniaxial fatigue loading. However, residual stiffness is highly sensible to measuring devices and calculating methods. A consistent decrease of stiffness during fatigue loading as expected could not be obtained. Depending on the range of R-ratios and loading direction relative to the grain, the observed residual stiffness seems to follow different trends.

Determining the appropriate failure criteria in fatigue life modeling poses challenges. The traditional approaches of S–N curves are incapable of capturing the influence of important fatigue parameters such as R-ratios and frequencies. Several investigations attempt to explore the interplay between creep and fatigue. The duration of load (DOL) criterion proves to be applicable to fatigue loading with a frequency of 0.1 Hz and less. Compared to residual stiffness, the fatigue modulus seems to be a more promising damage indicator to establish progressive fatigue life models. However, due to the microcracking behaviors present in tension, models based on fatigue modulus show unsatisfying fit to test results. The energy dissipation density reflects the combination of stress level, load waveform, loading frequency and material properties, which can be potentially used as a failure criterion in fatigue life predictions.

The fracture morphology and failure mechanisms of wood under cyclic loading can be explained through microscopic studies and physical observations. Fiber buckling and subsequent damage accumulation are identified as primary failure mechanisms for bending, influenced by stress redistribution and stress levels. The microstructure failure under compressive fatigue stress shares similarities with that under creep stress: the number of microscopic kinks in both cases is quantitatively related to accumulated strain. More efforts need to be taken to monitor microstructural damage during high cycle fatigue under tension and compression for a deeper understanding of the failure mechanism of wood in fatigue.

Declaration of competing interest

The authors declare that they have no known competing financial interests or personal relationships that could have appeared to influence the work reported in this paper.

Acknowledgments

This study was partially funded by the German Federal Ministry of Food and Agriculture through the Fachagentur Nachwachsende Rohstoffe e.V. (FNR) (grant number 22009817, HS-Hybrid project). The authors gratefully acknowledge the support of the Bavarian State Ministry of Food, Agriculture and Forestry in the WoodVibes project (grant number: LWF-A9-7831-26-4-1).

Appendix. Literature summary

Literature	Loading	Direction	Species Hardwood	Species Softwood	Specimen Type	Frequency	NOC	SL	Wave form	R	T	R.H./MC	Test Control
[28]	4-point bending	Parallel	Walnut, Ash	Pine heartwood, Pine sapwood, Spruce	Solid wood	50 Hz	1.00E+07	30%–70%	sin	−1		55% RH	Load Control
[29,49,76]	Bending	Parallel	Ash		Solid wood	–	1.00E+07		sin	−1			
[30]	3-point Bending	Parallel	Beech		LVL, Plywood	20, 2 Hz	2.00E+07	25%–80%			20 °C	65% RH	Displacement Control
[30]	Tension, Compression, 3-point Bending	Parallel	Beech		LVL	20, 2 Hz	2.00E+07	50%–80%			20 °C	65% RH	Displacement Control
[31]	Cantilever		Birch		Plywood, LVL	29 Hz	3.00E+06	20%–90%		−1			Load Control
[37]	4-point bending		Hard maple, Yellow birch		Solid wood, LVL, LVL (treated), Presswood, Presswood (treated)	57.5, 176.7 Hz	1.00E+08	15%–60%	sin	−1		1.6-8.0% MC	Load Control
[58]	Tension	Parallel	Determa Cedro, Kaneelhart, Timbauba, Hickory, Manni	Ceiba, Redwood, White pine	Solid wood	0.001 - 0.005 Hz (0.76 mm/min)	100	30%–80%		0	32 °C	9%–13% MC	Load Control
[32]	Cantilever		Yellow birch, Yellow poplar	Sitka spruce, Douglas fir	Solid wood, Plywood	29.8 Hz	5.00E+06	26%–80%		0, −1	24 °C	12% MC	Displacement Control
[51]	Tension				Particle board 1, Particle board 2, Particle board 3	43.3 Hz	3.00E+07	40%–70%	sin	>0 ,−1	23 °C	50% RH 10.2–11.5% MC	Load Control
[51]	Bending				Particle board 1, Particle board 2, Particle board 3	20 Hz	3.00E+07	20%–50%		>0 ,−1	23 °C	50% RH 10.2–11.5% MC	Displacement Control
[38]	Tension		Beech, Poplar	Pine, Douglas fir	Solid wood	25 Hz	2.50E+06	30-80 Mpa	sin	0		12% MC	Load Control
[38]	3-point Bending		Beech, Poplar	Pine, Douglas fir	Solid wood	25 Hz	2.50E+06	35-85 Mpa	sin	0		12% MC	Load Control
[8]	4-point bending	Parallel, 1:12 slope		Southern pine, Douglas fir	Quarter-scale bridge strianglenger (with/without treatment)	8.3 Hz	1.00E+07	35%–70%			24 °C	air dry (10%–11% MC), green(70%–80% RH)	Load Control
[77]	4-point bending			Spruce	Glulam beam (4 adhesives)	5.5 Hz	1.00E+07	55%–80%		>0	21 °C	12% MC 65% RH	Load Control
[9]	Torsion	Parallel	Shorea robusta, Terminalia Belerica, Dalbergia latifolia, Bambusa nutans, Tectona grandis	Cedrus deodara, Pinus insularis	Solid wood	23.7 Hz	2.00E+07	10%–55%				10%–40% MC	Displacement Control
[41]	Compression			Pine	Solid wood	40 Hz	3.50E+06	30%–80%	sin	>0	60, 40, 20, -10 °C	standard: 13% MC variational: 3%–24% MC	Load Control
[41]	Tension			Pine	Solid wood	40 Hz	3.50E+06	40%–60%	sin	>0	60, 40, 20, −10 °C	standard: 13% MC variational: 3%–24% MC	Load Control
[78]	Edgewise bending	Parallel, Perpendicular		Cedrus deodara	Solid wood	23.7 Hz	5.00E+07	25%–85%		−1		9%–15% MC	Displacement Control
[79]	4-point bending				Particleboard (pine) Glulam (beech), Glulam (Macore), Glulam (Limba)	/1 week, /1 month	75	40%–90%		0.5		9.4-11.4% MC	Load Control

Literature	Loading	Direction	Species Hardwood	Species Softwood	Specimen Type	Frequency	NOC	SL	Wave form	R	T	R.H./MC	Test Control
[59,80]	Tension	Parallel	Red beech		Solid wood	35 Hz	3.00E+06		sin	>0	30 °C	15.5% MC	Displace-ment Control
[81]	Tension	Parallel			Solid wood Finger Joint	15 Hz	3.00E+07	40%–90%		0.1	23.3 °C	12% MC 64% RH	Load Control
[75]	Compres-sion	Parallel	Ash		Solid wood	/5min	8	8.8 Mpa	square	∞	20 °C	12% MC 65% RH	Load Control
[75]	Compres-sion	Perpendic-ular	Ash		Solid wood	/5min	8	1.5 Mpa	square	∞	20 °C	12% MC 65% RH	Load Control
[42]	Tension	Parallel		Pine	Solid wood	–	2.20E+06	36%	sin	0	20-50 °C	7%–24% MC	Load Control
[42]	Compres-sion	Parallel		Pine	Solid wood	–	2.20E+06	50%	sin	∞	20-51 °C	7%–24% MC	Load Control
[42]	3-point Bending	Parallel		Pine	Solid wood	–	1.85E+06	50%	sin	−1	20-52 °C	7%–24% MC	Displace-ment Control
[42]	Compres-sion	Parallel		Pine	Solid wood	0.1, 0.01, 0.001, 0.0001, 0.00001, 0.000001 Hz	1−3000	74, 80, 86%	square	∞	20 °C	15% MC 75% RH	Load Control
[82]	Tension Compres-sion			Sitka spruce	Solid wood (butt-joint with metal connector)	1.67, 16.7 Hz	3.00E+07	20%–75%	sin	0, −1		12% MC	Load Control
[83]	Tension Compres-sion	Perpendic-ular	Sipo		Curved glulam	1 Hz	2.00E+06						
[84]	Tension			Western hemlock	Solid wood (butt-joint with metal connector)	16.7 Hz	–	25%–68%	sin	0		12% MC	Load Control
[53]	Compres-sion	Parallel		Sitka spruce	Solid wood	0.1, 10 Hz	1.00E+06	80%–125%	sin	∞	20 °C	12% MC	Load Control
[53]	Tension	Parallel		Sitka spruce	Solid wood	0.1, 10 Hz	1.00E+06	60%–100%	sin	0	20 °C	12% MC	Load Control
[85]	Tension	Perpendic-ular to surface			Particle board (3 adhesives)	10 Hz	1.00E+07	20%–90%	sin	0	25 °C	65% RH	Load Control
[86]	3-point Bending				Particle board 1, Particle board 2, Particle board 3, Particle board 4	1 Hz	1.00E+05	65%–95%		0	25 °C	65% RH	Load Control
[87]	Tension Compres-sion			douglas fir	Plywood, Plywood (scarf joint)	5 Hz	1.00E+07			0, −1, 0.5	48.9, 21 °C	17% MC 100%, 50% RH	Load Control
[88]	Tension	Perpendic-ular to surface			Particle board (3 adhesives)	10 Hz	1.00E+06	40%–100%	sin	0	25 °C	4%, 16% MC 65% RH	
[89]	Tension	Parallel		Sitka spruce	Solid wood	0.5 Hz	High cycle	10%–60%	sin tri-angle square	0	20 °C	12% MC	Load Control
[56]	Tension	Parallel		Sitka spruce	Solid wood	1 Hz	1.00E+05	60%–90%	sin tri-angle square	0	20 °C	12% MC	Load Control
[40]	Tension	Parallel		Sitka spruce	Solid wood	1 Hz	4.00E+02	30%–90%	sin tri-angle square	0	20 °C	12% MC	Load Control
[90]	Shear Test			hem-fir	Plywood, Particleboard (full-size shear wall panel)	0.003 Hz	≤200	30%–80%		−1		12%–15% MC	Load Control
[91]	Shear Test		Launan	hem-fir	Plywood, Particleboard, Hardboard, Nailed Joint	0.05, 0.1, 0.5, 1, 2 Hz	1.00E+05	20%–70%		−1			Load Control
[92]	4-point bending	Parallel		Agathis	Notched specimen	30 Hz	1.00E+06			−1		12% MC	Load Control
[93]	3-point Bending		Sugi	Hemlock	LVL with buttjoint (4 adhesives)	10 Hz	1.00E+06	60%–90%	sin	0	25 °C	8%–12% MC	Load Control
[3]	4-point bending		Khaya		LVL	1000MPa/s (15 Hz)	1.00E+07			0.1, 0.3, 0.5, −0.5, −1		5, 11, 35% MC	Load Control
[3]	4-point bending		Densified beech		LVL, Plywood	2600MPa/s (20 Hz)	1.00E+07			0.1		8% MC	Load Control

Literature	Loading	Direction	Species Hardwood	Species Softwood	Specimen Type	Frequency	NOC	SL	Wave form	R	T	R.H./MC	Test Control
[3]	4-point bending			sitka spruce	Solid wood	1600MPa/s	1.00E+07			0.1		12% MC	Load Control
[4]	Tension Compression	Parallel	Khaya	Douglas fir	LVL	200MPa/s	1.00E+07	30%–90%	sin	−1, −2, −10, 10, 0.1	20 °C		Load Control
[4]	Shear Test		Khaya		LVL	200MPa/s	1.00E+07	50%–90%	sin	0.1	20 °C		Load Control
[94]	4-point bending	Parallel 3, 6, 12 deg			Glulam	10 Hz	2.00E+06					12% MC	Displacement Control
[71]	4-point bending	Parallel		Sitka spruce	Solid wood	0.1, 1 Hz	1.00E+06	70%–100%	square	0	25 °C	12% MC	Load Control
[95]	Tension		Zelkova	Sitka spruce	Solid wood	1 Hz	1.00E+05	50%–90%	sin square	0	20 °C	12% MC	Load Control
[73]	Tension	Parallel	Japanese beech	Sitka spruce, Fir, Hemlock, Japanese cypress, Japanese larch	Solid wood	1 Hz	1.00E+06		sin square	0	25 °C	12% MC	Load Control
[72]	Tension	Parallel		Sitka spruce	Solid wood	1 Hz	1.00E+06	0%–20%	sin square	0	25 °C	12% MC	Load Control
[96]	Edgewise bending				MDF, OSB, Plywood	20 Hz	1.20E+06	30, 40, 50, 60, 70%					Load Control
[48]	4-point bending				Chipboard	1.2 MPa/s, 12 MPa/s, 150 MPa/s	1.00E+07	20, 30, 40, 50, 60, 70, 80%	sin	0.1	20 °C		Load Control
[97]	4-point bending				OSB, Chipboard, MDF	0.17 - 1.7 Hz	1.00E+06	20, 30, 40, 50, 60, 70, 81%	sin	0.1	25 °C	65% RH	Load Control
[98]	Tension Compression	Parallel		Spruce	Solid wood (joints with steel plates)	3, 6, 12, 25 Hz	1.00E+07		sin	0.1, −1	20 °C		Load Control
[74]	4-point bending	Parallel		Spruce	Solid wood	0.1, 1 Hz	1.00E+06	80%	square				Load Control
[39]	Cantilever		Japanese ash	Yezo (spruce)	Solid wood	–	1.00E+06				12, 13 °C	65% RH	Load Control
[65]	Tension Compression	Parallel	Khaya, Poplar, Beech		LVL	400 Mpa/s	1.00E+07	50,95%		3, −1, −3, −0.84, 0.33		65% RH	Load Control
[99]	Tension	Parallel Perpendicular		Spruce, Fir	Solid wood (bolted joints)	1, 5 Hz	1.00E+04	921	sin	0.1	20 °C	10% MC	Load Control
[100]	Tension	Parallel			Solid wood (bolted joints)	8.3 Hz	4.40E+07	95%					Load Control
[43]	Compression	Parallel		Spruce	Solid wood	0.01, 1, 10 Hz	22 000	80%	square		25 °C	65, 85%RH	Load Control
[63]	Compression	Parallel		Dark Spruce	Solid wood	0.5 Hz	120	90%	square		25 °C		Load Control
[50]	Tension, Compression	Parallel	Khaya		Khaya veneer	4, 7 Hz	1.00E+07	30%–80%	sin	0.1, 10, −1	20–25 °C	65% RH	Load Control
[101]	4-point bending			Douglas Fir, Pine	Full scale stringers	3 Hz	1.00E+07	50, 95%				19% MC	Load Control
[102]	Tension	Perpendicular		Spruce (Picea abies)	Solid wood	0.01, 1 Hz	1.00E+06	50, 65%	square			65, 85% RH	Load Control
[103]	4-point bending				OSB, Chipboard, MDF	0.17–1.7 Hz	1.00E+06	20, 30, 40, 50, 60, 70, 81%	sin	0.1	25 °C	65% RH	Load Control
[57]	Compression	Parallel		Dark Spruce	Solid wood	0.5 Hz	120	20,40, 60,80%	sin, triangle, square		20 °C	14.5% MC	Load Control
[17]	Tension	Parallel			LVL and Glulam/Pull-out of GFRP bolt	1–3.20 Hz	1.00E+06	80, 75, 50, 40, 25%	sin	0.1	25 °C	12% MC	Load Control
[10]	Tension			Japanese cypress	Solid wood	1 Hz	1.00E+06	100, 90, 80, 70, 60, 50%	triangle		25 °C	40% RH	Load Control
[60]	Compression	Parallel		Dark Spruce	Solid wood	0.2 Hz	120	100, 90, 80, 70, 60, 50%	triangle		20 °C	75% RH	Load Control

Literature	Loading	Direction	Species Hardwood	Species Softwood	Specimen Type	Frequency	NOC	SL	Wave form	R	T	R.H./MC	Test Control
[104]	Tension Compression			Douglas-fir	Solid wood/OSB sheet Nailed connection between OSB sheet and Douglas-fir lumber	0.2 Hz	38, 32, 30				20 °C	12% MC	Displacement Control
[11]	Axial and torsional load	Parallel		Japanese cypress	Solid wood	1 Hz	1.00E+06	100, 90, 80, 70, 60, 50%	triangle		25 °C	40% RH	Load Control
[105]	4-point bending				MDF, OSB, Chipboard	0.17 - 1.7 Hz	1.00E+06	80, 70, 60 50, 40%	triangle	0.1	25 °C	65% RH	Load Control
[12]	Torsion	Parallel Perpendicular 0, 45, 90°	Red Lauan	Sitka Spruce	Solid wood	0.17	70, 350	90, 80, 70, 50, 30%	triangle	0			Load Control
[18]	Tension		Red maple		LVL phenolic (FRP) composite bonded	1	–		sin	0.1, 0.3, 0.5	25 °C		Load Control
[13]	Shear Test	Parallel		Russian larch	plywood/Alkali phenol resin glue	0.5, 5 Hz	1.00E+07	50, 70, 90%	triangle		24 °C	55% RH	Load Control
[14]	Shear Test	Parallel		Russian larch	plywood/Alkali phenol resin glue	0.5, 5 Hz	1.00E+07	50, 70, 90%	triangle square		24 °C	55% RH	Load Control
[106]	Tension	Perpendicular		Norway spruce	Solid wood	1, 0.1, 0.01 Hz	1.00E+04	50, 65%	square		20 °C	12%–16% MC 65, 85%RH	Load Control
[107]	Tension Compression	Parallel		Pine	Glulam	6.5 Hz	2.00E+06		sin		20 °C		Displacement Control
[19]	4-point bending				Solid wood/finger jointed lumber	1.5, 2, 3.3 Hz	2.00E+06	30%–55%	sin	0.5	20 °C - 24 °C	40% - 53% RH	Load Control
[20]	Combined	Parallel	White ash, hickory		Solid wood/nailed joint	0.5 Hz	Low cycle	85%	sin		20 °C	65% RH 12% MC	Load Control
[54]	3-point Bending			Japanese cedar	Solid wood	0.5, 2.0, 5.0 Hz	1.00E+07	95, 85, 75, 65%	triangle square	0	20 °C	10.5 ± 1.31% MC	Load Control
[55]	3-point Bending		Selangan batu	Japanese cedar	Solid wood	0.5, 5.0 Hz	1.00E+07	70%–110%	triangle	0		11,12% MC	Load Control
[108]	3-point Bending		Beech	Scots pine	Solid wood	2 Hz	1.00E+06	80, 70, 60, 50, 40%	triangle		20 ± 2 °C	65 ± 5% RH	Load Control
[15]	Shear Test				CLT	–	281, 212		trapezoidal				Load Control
[61]	Tension	Parallel Perpendicular 10° slope	Beech		Solid wood/double-lap joint	5 Hz	1.00E+06	50, 70, 80%	triangle	−1	22 °C	50% RH	Load Control
[52]	3-point Bending	Parallel		Scots pine	Solid wood	20 Hz	1000, 505 000, 1 000 000	30%	sin	0.3	20 °C	35, 65 and 95% RH	Load Control
[109]	Tension Compression				Solid wood	2 Hz	1.00E+06			0.3			Displacement Control
[22]	Tensile shear		Beech		Solid wood/Lap joint	1 Hz	1.00E+06	45, 75%	sin		23 °C	50% RH	Load Control
[47]	Compression	Perpendicular		Japanese cypress	Solid wood	1 Hz	864 000	60%	triangle	0.01	25 °C	9.1 ± 0.5% MC	Load Control
[110]	4-point bending		Beech		Glulam (3 adhesives)	5 Hz	4.00E+04		triangle		20 °C	65% RH	Displacement Control
[111]	4-point bending	Parallel		Spruce	Wooden window frame with aluminium reinforcement	0.1 mm/s	5.00E+05	7.3–8.7 kN		0			Load Control
[112]	Compression	Parallel	Oak, Birch	Spruce	Solid wood	0.1 kN/s	(increasing amplitude test until failure)					absolute dry, fiber saturation	Load Control
[113]	3-point Bending		Beech	Pine	Resin modified wood	10 Hz	1.00E+06	50%–95%		0	20 °C	65% RH	Load Control

Literature	Loading	Direction	Species Hardwood	Species Softwood	Specimen Type	Frequency	NOC	SL	Wave form	R	T	R.H./MC	Test Control
[114]	3-point Bending		Caixeta, Cedroarana, Cambará, Tatajuba, Roxinho		Solid wood	0.5, 1 Hz	450, 4500, 45 000						Displacement Control
[25]	Cantilever		Ash	Scots pine	Heat-treated wood (L-shaped joints with plates)	0.33 Hz	1.75E+05				20 °C	65% RH	Load Control
[115]	Tension		Birch		Solid wood	20 000, 50 Hz	1.00E+09	36%	sin	−1	20 °C	65% RH	Load Control
[36]	3-point Bending	Tangential Radial		Norway Spruce	Solid wood	1 Hz	1.00E+07	50%	triangle	0	20 °C	65% RH	Load Control
[116]	Tension	Perpendicular	Maple		Solid wood	50 Hz	1.00E+09	75, 54%	sin	0.1, −1, 10	20 °C	65% RH	Load Control

References

[1] Barlow MT. The weight of aircraft: Characteristics and influences affecting aircraft weight, and possible development with increased size. Aircr Eng Aerosp Technol 1929;1(1):29–36. http://dx.doi.org/10.1108/00022669910370708.

[2] Kyanka GH. Fatigue properties of wood and wood composites. Int J Fract 1980;16(6):609–16. http://dx.doi.org/10.1007/BF02265220.

[3] Tsai KT, Ansell MP. The fatigue properties of wood in flexure. J Mater Sci 1990;25(2):865–78. http://dx.doi.org/10.1007/BF03372174.

[4] Ansell MP. Fatigue of wood and wood panel products. In: Fatigue in composites: science and technology of the fatigue response of fibre-reinforced plastics. North America: Woodhead Publishing Limited; 2003, p. 388–413.

[5] Bonfield PW, Ansell MP. Fatigue properties of wood in tension, compression and shear. J Mater Sci 1991;26(17):4765–73. http://dx.doi.org/10.1007/BF00612416.

[6] Van de Kuilen JW. Fatigue of timber and timber joints. 2004.

[7] Smith I, Landis E, Gong M. Fracture and fatigue in wood. Chichester, West Sussex, England ; Hoboken, NJ: J. Wiley; 2003.

[8] Gong M. Failure of spruce under compressive low-cycle fatigue loading parallel to grain [Ph.D. thesis], Canada: The University of New Brunswick; 2002.

[9] Lewis WC. Fatigue Resistance of quarter-scale bridge stringers in flexure and shear. Tech. rep, Forest Products Laboratory; 1962.

[10] Sekhar A, Schukla N, Gupta V. Einfluss von Torsionsspannungen und feuchtigkeit auf die dauerfestigkeitseigenschaften des holzes. Holz Als Roh- Und Werkst 1964;22:264–6.

[11] Sasaki, Yamasaki M. Effect of pulsating tension-torsion combined loading on fatigue behavior in wood. Holzforschung 2004;58(6):666–72. http://dx.doi.org/10.1515/HF.2004.121.

[12] Sasaki Y, Yamasaki M, Sugimoto T. Fatigue damage in wood under pulsating multiaxial-combined loading. Wood Fiber Sci 2005;37.

[13] Chen Z, Gabbitas B, Hunt D. The fracture of wood under torsional loading. J Mater Sci 2006;41(21):7247–59. http://dx.doi.org/10.1007/s10853-006-0913-y.

[14] Sugimoto T, Sasaki Y. Effect of loading frequency on fatigue life and dissipated energy of structural plywood under panel shear load. Wood Sci Technol 2006;40(6):501–15. http://dx.doi.org/10.1007/s00226-006-0080-y.

[15] Sugimoto T, Sasaki Y, Yamasaki M. Fatigue of structural plywood under cyclic shear through thickness I: Fatigue process and failure criterion based on strain energy. J Wood Sci 2007;53(4):296–302. http://dx.doi.org/10.1007/s10086-006-0864-6.

[16] Li Y, Lam F. Low cycle fatigue tests and damage accumulation models on the rolling shear strength of cross-laminated timber. J Wood Sci 2016;62(3):251–62. http://dx.doi.org/10.1007/s10086-016-1547-6.

[17] Madhoushi M, Ansell MP. Experimental study of static and fatigue strengths of pultruded GFRP rods bonded into LVL and glulam. Int J Adhes Adhes 2004;24(4):319–25. http://dx.doi.org/10.1016/j.ijadhadh.2003.07.004.

[18] Jia J, Davalos JF. An artificial neural network for the fatigue study of bonded FRP–wood interfaces. Compos Struct 2006;74(1):106–14. http://dx.doi.org/10.1016/j.compstruct.2005.03.012.

[19] Aicher S, Stapf G. Fatigue behaviour of finger jointed lumber. In: International council for research and innovation in building and construction. Germany; 2010.

[20] Li L, Gong M, Smith I, Li D. Exploratory study on fatigue behaviour of laterally loaded, nailed timber joints, based on a dissipated energy criterion. Holzforschung 2012;66(7):863–9. http://dx.doi.org/10.1515/hf-2011-0077.

[21] Ammann S, Niemz P. Fibre and adhesive bridging at glue joints in European beech wood. Wood Res 2014;59.

[22] Bachtiar EV, Clerc G, Brunner AJ, Kaliske M, Niemz P. Static and dynamic tensile shear test of glued lap wooden joint with four different types of adhesives. Holzforschung 2017;71(5):391–6. http://dx.doi.org/10.1515/hf-2016-0154.

[23] Clerc G. Analysis of the fatigue performance of adhesively bonded wood joints [Ph.D. thesis], Munich, Germany: Technical University of Munich; 2020.

[24] Karlsson E, Lindvall S. Fatigue performance on adhesive joints of timber wind turbine [Ph.D. thesis], Göteborg, Sweden: Chalmers University of Technology; 2020.

[25] Demirel S, Sen Er R. Evaluation and comparison of control and heat treated L-shape furniture joints produced from Scotch pine and ash wood under static bending and cyclic fatigue bending loadings. Maderas Cienc Tecnolí A 2022;24. http://dx.doi.org/10.4067/S0718-221X2022000100420.

[26] European Committee for Standardization. EN 1995-2-2: Eurocode 5 – Design of timber structures – Part 2: Bridges, Annex A. 2004.

[27] Malo KA, Massaro FM, Stamatopoulos H. Exploring fatigue rules for timber structures in Eurocode 5. In: Conference proceedings of the 4th international conference on timber bridges. Biel/Bienne, Switzerland: Berner Fachhochschule; 2022, http://dx.doi.org/10.24451/GGXV-H219.

[28] Kraemer O. Dauerbiegeversuche Mit Hölzern. Tech. rep, Verlag von R. Oldenbourg; 1930.

[29] Kollmann F. Die Esche und ihr Holz. Springer Berlin Heidelberg; 1941, http://dx.doi.org/10.1007/978-3-642-90915-3.

[30] Küch W. Zeit- und Dauerfestigkeit von Lagenhölzern. Holz Als Roh- Und Werkst 1942;5(2–3):69–73. http://dx.doi.org/10.1007/BF02605310.

[31] Dietz AGH, Grinsfelder H. Behavior of plywood under repeated stresses. J Fluids Eng 1943;65(3):187–91. http://dx.doi.org/10.1115/1.4018732.

[32] Kommers WJ. The fatigue behavior of wood and plywood subjected to repeated and reversed bending stresses (1327). 1960.

[33] Lewis WC. Design considerations for fatigue in timber structures. J Struct Div 1960;86(5):15–23. http://dx.doi.org/10.1061/JSDEAG.0000519.

[34] Sarkani S, Mazzuchi T, Lewandowski D, Kihl D. Runout analysis in fatigue investigation. Eng Fract Mech 2007;74(18):2971–80. http://dx.doi.org/10.1016/j.engfracmech.2006.08.026.

[35] Dean MA. Analysis of censored fatigue data. In: Proceeding of the 4th engineering mechanics division specialty conference, vol. 2. 1983, p. 919–22.

[36] Klemenc J, Fajdiga G. Statistical modelling of the fatigue bending strength of Norway spruce wood. Materials 2022;15(2):536. http://dx.doi.org/10.3390/ma15020536.

[37] Fuller FB, Oberg TT. Fatigue characteristics of natural and resin-impregnated, compressed, laminated woods. J Aeronaut Sci 1943;10(3):81–5. http://dx.doi.org/10.2514/8.10995.

[38] Gillwald VW. Beitrag zur bestimmung der formänderung von holz unter schwingender beanspruchung. Holz Als Roh- Und Werkst 1961;19(3):86–92.

[39] Nakano T. Fatigue and heating in the non-linear region for wood. Holzforschung 1997;51(4):309–15. http://dx.doi.org/10.1515/hfsg.1997.51.4.309.

[40] Okuyama T, Marsoem SN. Mechanical responses of wood to repeated loading IV: Temperature-rises due to energy loss. J Jpn Wood Res Soc 1987;33(11):844–50.

[41] Rose G. Das mechanische verhalten des kiefernholzes bei dynamischer dauerbeanspruchung in abhängigkeit von belastungsart, belastungsgröße, feuchtigkeit und temperatur. Holz Als Roh- Und Werkst 1965;23(7):271–84. http://dx.doi.org/10.1007/BF02605242.

[42] Kufner VM. Änderung der festigkeit und des elastizitätsmoduls von kiefernholz infolge dauerbeanspruchung. Holz Als Roh- Und Werkst 1969;27:pages 261–270.

[43] Clorius CO, Pedersen MU, Hoffmeyer P, Damkilde L. Compressive fatigue in wood. Wood Sci Technol 2000;34(1):21–37. http://dx.doi.org/10.1007/s002260050005.

[44] Eide S, Nore K, Aasheim E. Research note: compression perpendicular to the grain – the norwegian approach. Tech. rep, 2011.

[45] Hunt DG. A unified approach to creep of wood. Proc R Soc Lond Ser A Math Phys Eng Sci 1999;455(1991):4077–95. http://dx.doi.org/10.1098/rspa.1999.0491.

[46] Bach L. Frequency-dependent fracture in wood under pulsating loading. 1975.

[47] Ogawa K, Shimizu K, Yamasaki M, Sasaki Y. Fatigue behavior of Japanese cypress (*Chamaecyparis Obtusa*) under repeated compression loading tests perpendicular to the grain. Holzforschung 2017;71(6):499–504. http://dx.doi.org/10.1515/hf-2016-0227.

[48] Thompson R, Bonfield P, Dinwoodie J, Ansell M. Fatigue and creep in chipboard: Part 3. The effect of frequency. Wood Sci Technol 1996;30(5). http://dx.doi.org/10.1007/BF00223550.

[49] Kollmann F. Zeit und Festigkeit. Holz- Zentralblatt: UnabhÄ Ngiges Organ Die Forst- Und Holzwirtsch 1959;85(139/140):1867–9.

[50] Hacker CL, Ansell MP. Fatigue damage and hysteresis in wood-epoxy laminates. J Mater Sci 2001;36:609–21.

[51] Kollmann F, Krech H. Zeitfestigkeit und Dauerfestigkeit von Holzspanplatten. Holz Als Roh- Und Werkst 1961;19(3):113–8. http://dx.doi.org/10.1007/BF02609523.

[52] Sharapov E, Mahnert K-C, Militz H. Residual strength of thermally modified Scots pine after fatigue testing in flexure. Eur J Wood Wood Prod 2016;74(6):875–84. http://dx.doi.org/10.1007/s00107-016-1082-6.

[53] Okuyama T, Itoh, Marsoem SN. Mechanical responses of wood to repeated loading I: Tensile and compressive fatigue fractures. J Jpn Wood Res Soc 1984;30(10):791–8.

[54] Sasaki Y, Oya A, Yamasaki M. Energetic investigation of the fatigue of wood. Holzforschung 2014;68(7):843–8. http://dx.doi.org/10.1515/hf-2013-0147.

[55] Watanabe A, Sasaki Y, Yamasaki M. Bending fatigue of wood; strain energy-based failure criterion and fatigue life prediction. Wood Fiber Sci 2014;46.

[56] Marsoem SN, Bordonne P, Okuyama T. Mechanical responses of wood to repeated loading II: Effect of wave-form on tensile fatigue. J Jpn Wood Res Soc 1987;33(5):354–60.

[57] Gong M, Smith I. Effect of waveform and loading sequence on low-cycle compressive fatigue life of spruce. J Mater Civ Eng 2003;15(1):93–9. http://dx.doi.org/10.1061/(ASCE)0899-1561(2003)15:1(93).

[58] Sterr R. Untersuchungen zur Dauerfestigkeit von Schichtholzbalken. Holz Als Roh- Und Werkst 1963;21(2):47–61. http://dx.doi.org/10.1007/BF02609715.

[59] Kellogg R. Effect of repeated loading on tensile properties of wood. For Prod J 1960;10(11):586–94.

[60] Noack D, Stöckmann V. Prinzip der dauerschwingbeanspruchung als statischer relaxationsversuch mit überlagerter dynamischer relaxation. Holz Als Roh- Und Werkst 1968;26:447–53.

[61] Gong M, Smith I. Effect of stress levels on compressive low-cycle fatigue behaviour of softwood. Holzforschung 2005;59(6):662–8. http://dx.doi.org/10.1515/HF.2005.106.

[62] Myslicki S, Vallée T, Walther F. Short-time procedure for fatigue assessment of beech wood and adhesively bonded beech wood joints. Mater Struct 2016;49(6):2161–70. http://dx.doi.org/10.1617/s11527-015-0640-4.

[63] Launay A, Maitournam M, Marco Y, Raoult I, Szmytka F. Cyclic behaviour of short glass fibre reinforced polyamide: experimental study and constitutive equations. Int J Plast 2011;27(8):1267–93. http://dx.doi.org/10.1016/j.ijplas.2011.02.005.

[64] Gong M, Smith I. Failure mechanism of softwood under low-cycle fatigue load in compression parallel to grain. 2000.

[65] Hacker CL. Fatigue damage in wood composites [Ph.D. thesis], University of Bath; 1995.

[66] Bond I, Ansell MP. Fatigue properties of jointed wood composites - Part I Statistical analysis, fatigue master curves and constant life diagrams. J Mater Sci 1998;33:2751–62.

[67] Gerhards CC, Link C. A cumulative damage model to predict load duration characteristics of lumber. Wood Fiber Sci 1987;19.

[68] Barrett JD, Foschi RO. Duration of load and probability of failure in wood. Part I. modelling creep rupture. Can J Civil Eng 1978;5(4):505–14. http://dx.doi.org/10.1139/l78-057.

[69] Yao FZ, Foschi RO. Duration of load in wood: Canadian results and implementation in reliability-based design. Can J Civil Eng 1993;20(3):358–65. http://dx.doi.org/10.1139/l93-050.

[70] van Der Put TACM. Deformation and damage processes in wood. Delft: Delft University; 1989.

[71] Krausz AS, Eyring H, Krausz AS. Deformation kinetics. A wiley-interscience publication, New York: Wiley; 1975.

[72] Kohara M, Okuyama T. Mechanical responses of wood to repeated loading V: Effect of duration time and number of repetitions on the time to failure in bending. J Jpn Wood Res Soc 1992;38(8):753–8.

[73] Kohara M, Okuyama T. Mechanical responses of wood to repeated loading VII: dependence of energy loss on stress amplitude and effect of wave forms on fatigue lifetime. J Jpn Wood Res Soc 1994;40(5):491–6.

[74] Kohara M, Okuyama T. Mechanical responses of wood to repeated loading VIII: variation of energy loss behaviors with species. J Jpn Wood Res Soc 1994;40(8):801–9.

[75] Kohara M, Kanayama K, Nakai A, Nagata K, Okuyama T. Damages in wood beams caused by fatigue under pulsating loads. J Jpn Wood Res Soc 1997;43(11):909–15.

[76] Curtu I, Paraschiv N, Fleischer H. Die verformung druckbeanspruchten eschenholzes in abhängigkeit von der probengröße. Holz Als Roh- Und Werkst 1969;27(2):49–54. http://dx.doi.org/10.1007/BF02612762.

[77] Kollmann F. Technologie des holzes und der holzwerkstoffe - anatomie und pathologie, chemie, physik elastizität und festigkeit. Berlin, Heidelberg: Springer Berlin Heidelberg; 1951, http://dx.doi.org/10.1007/978-3-642-49758-2, .

[78] Sekhar A, Schukla N. Der Einfluss von Faserrichtungswinkel Und Biegemoment Auf Die Dauerfestigkeit von Cedrus Deodara. Holz Als Roh- Und Werkst 1965;23:434–7.

[79] Möhler K, Ehlbeck J. Versuche über das Dauerstandverhalten von Spanplatten und Furnierplatten bei Biegebeanspruchung. Holz Als Roh- Und Werkst 1968;26:118–24.

[80] Noack D, Stöckmann V. Dauerschwingverhalten von Rotbuchenholz unter konstanten Temperatur- und Feuchtigkeitsbedingungen. Holz Als Roh- Und Werkst 1969;27:464–72.

[81] Bohannan B. Fatigue strength of finger joints. Tech. Rep 114, Forest Products Laboratory; 1969.

[82] Hayashi T, Sasaki H, Masuda M. Fatigue properties of wood butt joints with metal plate connectors. For Prod J 1980;30(2):49–53.

[83] von Roth W, Noack D. Untersuchungen zum Dauerschwingverhalten von Rahmenecken aus gekrümmtem lamelliertem Schichtholz. Holz Als Roh- Und Werkst 1983;41:233–40.

[84] Hayashi T, Sasaki H. Fatigue damage of wood butt-joints with metal plate connectors. J Jpn Wood Res Soc 1984;30(1):23–31.

[85] Suzuki S, Saito F. Fatigue behavior of particleboard in tension perpendicular to the surface I: Effect of resin type. J Jpn Wood Res Soc 1984;30(10):799–806.

[86] Tanaka A, Suzuki S. Bending fatigue strength of particleboard. J Jpn Wood Res Soc 1984;30(10):807–13.

[87] Johnson P. Design of test specimens and procedures for generating material properties of douglas fir/epoxy laminated wood composite material: With the generation of baseline data at two environmental conditions. Tech. Rep NASA CR-174910, Dayton, Ohio: University of Dayton Research Institute; 1985.

[88] Suzuki S, Saito F. Fatigue behavior of particleboard in tension perpendicular to the surface II: Effect of moisture content. J Jpn Wood Res Soc 1986;32(10):801–7.

[89] Bordonne P, Okuyama T, Marsoem SN. Mechanical responses of wood to repeated loading III: Effect of wave-form on dissipated energy. J Jpn Wood Res Soc 1987;33(8):623–9.

[90] Tokuda M. Prediction of the number of cycles to failure of nailed shear-wall panels under reversed cyclic loading. J Jpn Wood Res Soc 1987;33(7):558–63.

[91] Tokuda M. Fatigue properties of nailed joints under reversed cyclic loading. J Jpn Wood Res Soc 1987;33(7):605–9.

[92] Imayama N. The fatigue of wood VI: Fatigue crack-propagation of cracked specimens. J Jpn Wood Res Soc 1988;34(11):896–903.

[93] Hayashi T. Fatigue properties of structural laminated-veneer-lumber. J Jpn Wood Res Soc 1989;35(7):616–24.

[94] Hansen L. Experimental investigation of fatigue properties of laminated wood beams.pdf. In: Proceedings of the 1991 international timber engineering conference. 1991.

[95] Kohara M, Okuyama T. Mechanical responses of wood to repeated loading VI: Energy-loss partitioning scheme to predict tensile fatigue lifetime. J Jpn Wood Res Soc 1993;39(11):1226–30.

[96] Bao Z, Eckelman C, Gibson H. Fatigue strength and allowable design stresses for some wood composites used in furniture. Holz Als Roh- Und Werkst 1996;54(6):377–82. http://dx.doi.org/10.1007/s001070050204, .

[97] Thompson RJH. Fatigue and creep in wood based panel products [Ph.D. thesis], University of Bath; 1996.

[98] Aasheim E. Cyclic testing of joints with dowels and slotted-in steel plate. Tech. rep, Vancouver. Canada: Norwegian Institute of Wood Technology; 1997.

[99] Chaplain M, Valentin G. Lifetime of wood joints: Fracture mechanics and damage modelling. In: Proceedings of pacific timber engineering conference, vol. 3. 1999, p. 414–21.

[100] Pedersen MU, Clorius CO, Damkilde L, Hoffmeyer P. Strength of glued-in bolts after full-scale loading. J Perform Constr Facil 1999;13(3):107–13. http://dx.doi.org/10.1061/(ASCE)0887-3828(1999)13:3(107).

[101] Uppal AS, Otter DE, Fry GT, Comardo AF. Fatigue strength of treated douglas fir timber railroad bridge stringers. Tech. rep, Transportation Technology Center, Inc.; 2001.

[102] Clorius CO. Fatigue in wood: an investigation in tension perpendicular to the grain [Ph.D. thesis], Kgs. Lyngby, Denmark: Technical University of Denmark; 2002.

[103] Thompson RJH, Ansell MP, Bonfield PW, Dinwoodie JM. Fatigue in wood-based panels. part 1: the strength variability and fatigue performance of OSB, chipboard and MDF. Wood Sci Technol 2002;36(3):255–69. http://dx.doi.org/10.1007/s00226-001-0136-y.

[104] Kent SM, Leichti RJ, Rosowsky DV, Morrell JJ. Effects of decay on the cyclic properties of nailed connections. J Mater Civ Eng 2005;17(5):579–85. http://dx.doi.org/10.1061/(ASCE)0899-1561(2005)17:5(579).

[105] Thompson RJH, Ansell MP, Bonfield PW, Dinwoodie JM. Fatigue in wood-based panels. Part 2: Property changes during fatigue cycling of OSB, chipboard and MDF. Wood Sci Technol 2005;39(4):311–25. http://dx.doi.org/10.1007/s00226-004-0277-x.

[106] Clorius CO, Pedersen MU, Hoffmeyer P, Damkilde L. An experimentally validated fatigue model for wood subjected to tension perpendicular to the grain. Wood Sci Technol 2009;43(3–4):343–57. http://dx.doi.org/10.1007/s00226-009-0244-7.

[107] Nosti CJ. Performance analysis and life prediction for small wind turbind blades: A wood laminate case study [Ph.D. thesis], San Luis Obispo, California: California Polytechnic State University; 2009, http://dx.doi.org/10.15368/theses.2009.126.

[108] Yildirim MN, Uysal B, Ozcifci A, Ertas AH. Determination of fatigue and static strength of scots pine and beech wood. Tech. rep, Flensburg University of Applied Sciences Wind Energy Technology Institute; 2015.

[109] Zhang C, Liao H, Qian C, Li H, Song L, Zheng J. Tensile-compressive fatigue experiment of wood in ancient buildings. Eng Mech 2016;33:201–6. http://dx.doi.org/10.6052/j.issn.1000-4750.2015.05.S031.

[110] Clerc G, Brunner AJ, Josset S, Niemz P, Pichelin F, Van de Kuilen JWG. Adhesive wood joints under quasi-static and cyclic fatigue fracture mode II loads. Int J Fatigue 2019;123:40–52. http://dx.doi.org/10.1016/j.ijfatigue.2019.02.008.

[111] Fajdiga G, Rajh D, Vidic D, Gospodarič B. The development of pneumatic fatigue test rig for wood-based specimens. Forests 2020;11(11):1187. http://dx.doi.org/10.3390/f11111187.

[112] Dobrowolska E, Niedbała M, Tabaczyński D. Testing of the fatigue strength along wood fibres at different moisture contents. Ann WULS, For Wood Technol 2021;115:45–54. http://dx.doi.org/10.5604/01.3001.0015.5133.

[113] Pečnik JG, Kutnar A, Militz H, Schwarzkopf M, Schwager H. Fatigue behavior of beech and pine wood modified with low molecular weight phenol-formaldehyde resin. Holzforschung 2021;75(1):37–47. http://dx.doi.org/10.1515/hf-2020-0015, .

[114] Carvalho JS, Christoforo AL, Lahr FAR, Aquino VBDM. Effect of fatigue on tropical wood species. Ambient Construí Do 2022;22(2):187–98. http://dx.doi.org/10.1590/s1678-86212022000200600.

[115] Karr U, Fitzka M, Schönbauer BM, Krenke T, Müller U, Mayer H. Fatigue testing of wood up to one billion load cycles. Holzforschung 2022;76(11–12):977–84. http://dx.doi.org/10.1515/hf-2022-0111, .

[116] Schönbauer B, Killinger M, Karr U, Fitzka M, Müller U, Teischinger A, et al. Fatigue properties of wood at different load ratios tested at 50 Hz and 20 kHz. Mater Und Werkst 2022;53(3):344–54. http://dx.doi.org/10.1002/mawe.202100280.